Cholesterol Effects on the Physical Properties of Lipid Membranes Viewed by Solid-state NMR Spectroscopy

Trivikram R. Molugu and Michael F. Brown

Abstract In this chapter, we review the physical properties of lipid/cholesterol mixtures involving studies of model membranes using solid-state NMR spectroscopy. The approach allows one to quantify the average membrane structure, fluctuations, and elastic deformation upon cholesterol interaction. Emphasis is placed on understanding the membrane structural deformation and emergent fluctuations at an atomistic level. Lineshape measurements using solid-state NMR spectroscopy give equilibrium structural properties, while relaxation time measurements study the molecular dynamics over a wide timescale range. The equilibrium properties of glycerophospholipids, sphingolipids, and their binary and tertiary mixtures with cholesterol are accessible. Nonideal mixing of cholesterol with other lipids explains the occurrence of liquid-ordered domains. The entropic loss upon addition of cholesterol to sphingolipids is less than for glycerophospholipids, and may drive formation of lipid rafts. The functional dependence of ^{2}H NMR spin–lattice relaxation (R_{1Z}) rates on segmental order parameters (S_{CD}) for lipid membranes is indicative of emergent viscoelastic properties. Addition of cholesterol shows stiffening of the bilayer relative to the pure lipids and this effect is diminished for lanosterol. Opposite influences of cholesterol and detergents on collective dynamics and elasticity at an atomistic scale can potentially affect lipid raft formation in cellular membranes.

Keywords Area per lipid · Cholesterol · Lanosterol · Lipid rafts · Membrane elasticity · Solid-state NMR

T. R. Molugu
Department of Chemistry and Biochemistry, University of Arizona, Tucson, AZ, USA

M. F. Brown (✉)
Department of Chemistry and Biochemistry, University of Arizona, Tucson, AZ, USA

Department of Physics, University of Arizona, Tucson, AZ, USA
e-mail: mfbrown@u.arizona.edu

A. Rosenhouse-Dantsker, A. N. Bukiya (eds.), *Cholesterol Modulation of Protein Function*, Advances in Experimental Medicine and Biology 1115,
https://doi.org/10.1007/978-3-030-04278-3_5

1 Introduction

Cholesterol is an essential component of mammalian cells constituting up to about 50 mol% of the total lipids in the plasma membrane [1, 2]. It plays key roles in maintaining the membrane integrity and regulating cell permeability [3]. Cellular functions are modulated by cholesterol in two different ways: either indirectly by affecting membrane properties due to lipid-cholesterol interactions [4–7] or directly by cholesterol-protein interactions [8–10]. As a steroid molecule, cholesterol has four fused rings and a hydrocarbon chain, which are hydrophobic, and a polar hydroxyl group making it overall amphiphilic as for other lipids (Fig. 1). Due to its

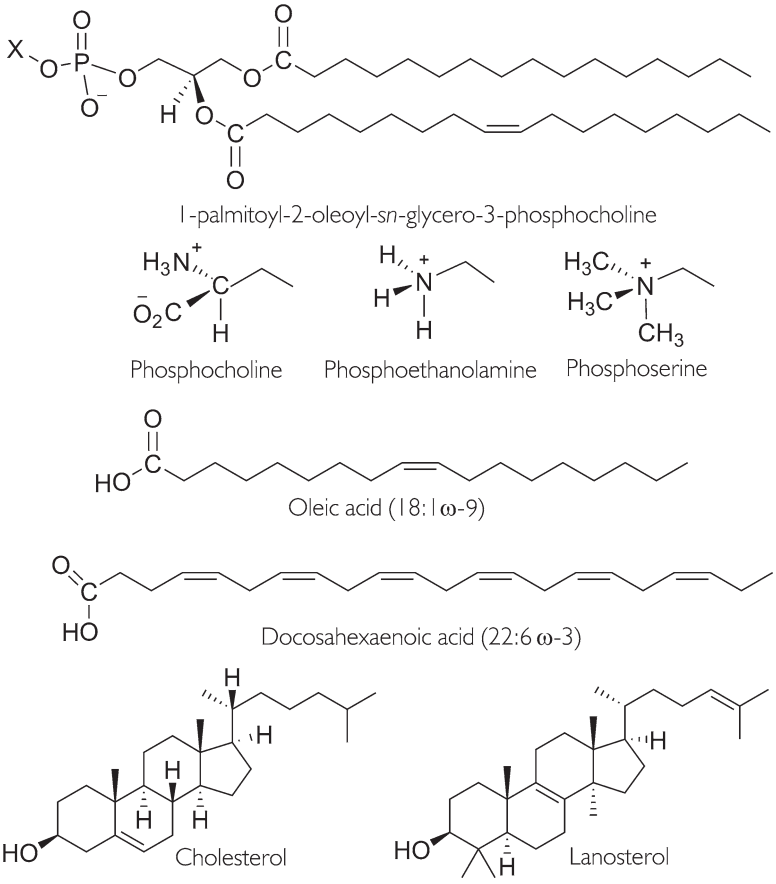

Fig. 1 Selected glycerophospholipid chemical structures, cholesterol, and lanosterol. The polar head groups vary in size, hydrogen bonding, and charge. Examples are shown for zwitterionic phosphocholine (PC) and phosphoethanolamine (PE) head groups, and for the anionic phosphoserine (PS) head group. Nonpolar acyl chains differ in length and degree of unsaturation, as illustrated by oleic acid (18:1ω-9) and docosahexaenoic acid (22:6ω-3). Cholesterol differs in the absence of methylation at the α-face relative to its biological precursor lanosterol. Figure adapted from [11]

chemical composition, most of the steroidal core structure fits into the lipid bilayer, with the fused rings in close proximity and interacting with the hydrocarbon chains of the lipids, while the polar hydroxyl group orients the molecule at the aqueous interface. When cholesterol is present in the liquid-ordered (l_o) phase, the lipid hydrocarbon chains become more ordered relative to the cholesterol-free (liquid-disordered, l_d) state. The lipid chain ordering induces alterations in the structural, dynamical [12], and physical properties of the lipid membrane, and thus can affect cellular signaling. The balance of attractive and repulsive forces for the membrane lipids is the consequence of both the polar headgroups and the nonpolar moieties, and yields a substantial polymorphism involving both lamellar and nonlamellar phases [13–20]. Notably, the structural and dynamical properties of biomembranes are mediated by the lipid composition and interactions with the proteins, water, cholesterol, and surfactants [7, 21–33]. Membrane remodeling requires mesoscopic elastic deformations of the lipids [30] that can play a central role in biological functioning with regard to lipid-protein interactions [6, 34, 35], domain formation, and various nano- and microstructures implicated in key cellular functions [34, 36–38]. Because the composition of lipids and cholesterol in cell membranes influences the lipid organization and membrane properties, it is not surprising that disorders in cellular cholesterol levels are implicated in various diseases [39, 40].

Many of the molecular species of lipids and proteins in membranes do not mix ideally [19, 20, 41–47]—cholesterol is one such component that is unequally distributed in cellular membranes, allowing for the presence of liquid-ordered raft-like domains [19, 20, 32, 42, 46–52]. Such raft-like domains have attracted considerable attention as platforms for signaling regulation in cellular biology and pharmacology [53–60]. The concept that biomembranes are homogeneous two-dimensional fluids with randomly distributed proteins (the fluid mosaic model) is challenged by the hypothesis that cellular membranes may contain such areas of lateral segregation [20, 55, 61–73]. By analysis of the liquid-ordered (l_o) phase [74, 75] and its possible connection with rafts in biological membranes [76, 77], the effect of cholesterol on domain formation in liquid-crystalline bilayers has been of great interest for membrane biophysicists [78]. For instance, raft-like domains are believed to occur in lipid systems with coexisting liquid-disordered (l_d) and liquid-ordered (l_o) phases. The l_d phase in these systems typically contains highly unsaturated lipids with a low phase-transition temperature, while the l_o phase predominantly consists of saturated glycerophospholipids or a sphingolipid component and cholesterol [2, 77]. Moreover, various proteins are endowed with the ability to interact with cholesterol via specific sensing mechanisms. The cholesterol recognition/interaction amino acid consensus (CRAC) sequence motif [79–82] is an example of such a recognition element. In some cases, they include cationic clusters that allow interactions with phosphatidylinositol 4,5-bisphosphate (PIP_2) in a cholesterol-dependent manner. Notably, such CRAC domains are found in the *Rhodopsin* (Family A) G-protein-coupled receptors (GPCRs) [83], and moreover posttranslational lipid modifications [84, 85] can promote sequestration into cholesterol-rich regions or microdomains.

Improving our understanding of complex lipid mixtures is an important aspect for current research in pharmacology, biophysics, and biochemistry as well as in

cellular biology. Various experimental methods have been used to study lipid–cholesterol interactions, including electron spin resonance (ESR) [86–94], Raman [95–97], Fourier transform infrared (FT-IR) [98, 99], and fluorescence spectroscopy [100–102]; atomic force microscopy (AFM) [103–105]; multidimensional nuclear magnetic resonance (NMR) spectroscopy [70, 73, 106, 107]; solid-state NMR spectroscopy [65, 101, 108–119]; and X-ray [72, 120, 121] and neutron diffraction methods [122–124]. Still, a thorough understanding of the physical basis for these observations in relation to the intricate lipid compositions of many biological membranes remains a conundrum [20, 51, 71, 125, 126]. This chapter covers recent developments in understanding lipid–cholesterol interactions in model membrane systems and implications for cellular function as seen by solid-state nuclear magnetic resonance (NMR) spectroscopy. First, we give a brief introduction to solid-state NMR methods for nonexperts to appreciate the results as applied to lipid-cholesterol systems. Next, we explain how solid-state NMR technology is applied for obtaining membrane structural and dynamical properties. We then discuss the sterol interactions with phospholipids in model membranes, including the role of configurational entropy in lipid raft formation. Emphasis is placed on how the average material properties emerge from the atomistic level interactions in lipid bilayers, as investigated by combining NMR spectroscopy with relaxation methods [11, 111, 112, 127].

2 Solid-State NMR Spectroscopy of Lipid Membranes

Solid-state NMR spectroscopy [29, 128–130] offers a versatile and noninvasive method for studying the molecular organization of lipids within membranes. In particular, isotopic substitution of ^{2}H for ^{1}H constitutes a minimal structural perturbation [131]. Interpretation of the ^{2}H NMR spectra is relatively straightforward, due to the intramolecular nature of the quadrupolar interaction that dominates the lineshape. There are a number of reviews that give a comprehensive treatment of ^{2}H NMR spectral analysis [30, 128, 129, 131–135]. An essential feature of ^{2}H NMR spectroscopy is that one introduces site-specific ^{2}H-labels, corresponding to the individual C–^{2}H bonds. In this way, we obtain atomistically resolved information for noncrystalline amorphous or liquid-crystalline systems. Because the coupling interactions in solid-state NMR are sensitive to orientation and/or distance, their values correspond to the average structure of the system of interest. On the other hand, molecular motions are manifested by the relaxation parameters that are also accessible in NMR spectroscopy. A unique feature is that in solid-state ^{2}H NMR of biomolecular systems, we acquire both lineshape data [118] and relaxation times [136] for investigating structural dynamics. Measurement of the ^{2}H NMR lineshapes yields knowledge of the average structure through the principal values of the coupling tensor as well as the principal axis system. Yet, if we only determine the coupling tensors, then the method mainly provides us with structural knowledge as in X-ray crystallography. An important feature of solid-state ^{2}H NMR spectroscopy

is that information is also obtained regarding the molecular motions, encompassing a range of different timescales. Through the combined measurement of residual quadrupolar couplings (RQCs) and relaxation rates, we thereby obtain knowledge of the geometry as well as investigate the multiscale molecular motions and their amplitudes in the membrane systems of interest. An analogous approach is introduced in the case of solid-state ^{13}C NMR spectroscopy of membrane lipids and biomembranes at natural isotopic abundance.

2.1 Deuterium Solid-State NMR Spectroscopy

Notably, ^{2}H NMR spectroscopy gives us a particularly simple illustration of the principles of magnetic resonance as applied to molecular solids, liquid crystals, and biomembranes. This is because the very large electric quadrupolar interaction dominates over the magnetic dipolar couplings of the ^{2}H and ^{1}H nuclei as well as the ^{2}H chemical shifts [134, 136]. The ^{2}H nucleus has a spin of $I = 1$, and hence there are three Zeeman energy levels due to projecting the nuclear spin angular momentum onto the magnetic field direction. The three eigenstates $|m\rangle = |0\rangle$ and $|\pm1\rangle$ are given by the Hamiltonian $\hat{H}_Z$ for interaction of the nuclear magnetic moment with the static magnetic field. We learn in quantum mechanics that the transitions between adjacent spin energy levels are allowed, which yields the two single-quantum nuclear spin transitions. Moreover, the degeneracy of the allowed transitions in ^{2}H NMR is removed by the quadrupolar coupling. Here, the perturbing Hamiltonian $\hat{H}_Q$ is due to interaction of the quadrupole moment of the ^{2}H nucleus with the electric field gradient (EFG) of the C–^{2}H bond. It follows that for each inequivalent site, two spectral branches are observed in the experimental spectrum.

In solid-state ^{2}H NMR spectroscopy, the experimentally observed quadrupolar coupling is given by the difference in the frequencies $\Delta\nu_Q^{\pm} \equiv \Delta\nu_Q^{+} - \Delta\nu_Q^{-}$ of the spectral lines due to the perturbing Hamiltonian. The result for the quadrupolar frequencies ($\nu_Q^{\pm}$) thus reads:

$$\nu_Q^{\pm} = \pm\frac{3}{4}\chi_Q\left\{D_{00}^{(2)}(\Omega_{PL}) - \frac{\eta_Q}{\sqrt{6}}\left[D_{-20}^{(2)}(\Omega_{PL}) + D_{20}^{(2)}(\Omega_{PL})\right]\right\}. \quad (1)$$

In the above formula, $\chi_Q \equiv e^2qQ/h$ is the *static* quadrupolar coupling constant, η_Q corresponds to the asymmetry parameter of the EFG tensor, $D_{00}^{(2)}(\Omega_{PL})$ is a Wigner rotation matrix element, and $\Omega_{PL} \equiv (\alpha_{PL}, \beta_{PL}, \gamma_{PN})$ are the Euler angles [137] relating the principal axis system (PAS) of the EFG tensor (P) to the laboratory frame (L) [29, 128, 136]. Furthermore, it turns out that the static EFG tensor of the C–^{2}H bond is nearly axially symmetric ($\eta_Q \approx 0$), which leads us to the simpler result:

$$\nu_Q^{\pm} = \pm\frac{3}{4}\chi_Q D_{00}^{(2)}(\Omega_{PL}). \quad (2)$$

The experimental quadrupolar splitting is thus given by:

$$\Delta\nu_{\mathrm{Q}} = \frac{3}{2}\chi_{\mathrm{Q}} D_{00}^{(2)}\left(\Omega_{\mathrm{PL}}\right). \tag{3}$$

Now in liquid-crystalline membranes, the motions of the constituent molecules are often cylindrically symmetric about the bilayer normal, an axis known as the director. The overall rotation of the principal axis system of the coupling tensor to the laboratory frame, described by the Ω_{PL} Euler angles, can thus be represented by the effect of two consecutive rotations. First, the Euler angles $\Omega_{\mathrm{PD}}(t)$ represent the (time-dependent) rotation from the principal axis frame to the director frame, and second the Euler angles Ω_{DL} represent the (static) rotation from the director frame to laboratory frame. Using the closure property of the rotation group [136], and considering the cylindrical symmetry about the director, we can then expand Eq. (3), which now reads

$$\Delta\nu_{\mathrm{Q}} = \frac{3}{2}\chi_{\mathrm{Q}}\left\langle D_{00}^{(2)}\left(\Omega_{\mathrm{PD}}\right)\right\rangle D_{00}^{(2)}\left(\Omega_{\mathrm{DL}}\right) \tag{4a}$$

$$= \frac{3}{2}\chi_{\mathrm{Q}}\frac{1}{2}\left\langle 3\cos^2\beta_{\mathrm{PD}} - 1\right\rangle \frac{1}{2}\left(3\cos^2\beta_{\mathrm{DL}} - 1\right). \tag{4b}$$

Here, $\beta_{\mathrm{DL}} \equiv \theta$ is the angle of the bilayer normal to the static external magnetic field. The segmental order parameter S_{CD} is given by:

$$S_{\mathrm{CD}} = \frac{1}{2}\left\langle 3\cos^2\beta_{\mathrm{PD}} - 1\right\rangle \tag{5}$$

where the angular brackets denote a time/ensemble average. It follows that

$$\Delta\nu_{\mathrm{Q}} = \frac{3}{2}\chi_{\mathrm{Q}} S_{\mathrm{CD}} P_2\left(\cos\beta_{\mathrm{DL}}\right) \tag{6}$$

where $P_2(\cos\beta_{\mathrm{DL}}) \equiv (3\cos^2\beta_{\mathrm{DL}} - 1)/2$ is the second-order Legendre polynomial. The above expression describes the dependence of the quadrupolar splitting on the (Euler) angles that rotate the coupling tensor from its principal axes system to the laboratory frame, as defined by the main magnetic field. Figure 2 illustrates the effect of cholesterol on the solid-state deuterium NMR lineshape for 1,2-diperdeuteriomyristoyl-*sn*-glycero-3-phosphocholine (DMPC-d_{54}) bilayers. A gradual increase in the quadrupolar splittings ($\Delta\nu_{\mathrm{Q}}$) for the acyl segments is observed as cholesterol concentration is increased, which reflects increased orientational order of the acyl chain segments with respect to the bilayer normal. This finding explains the well-known condensing effect of cholesterol at the molecular level, involving a reduction of the area per phospholipid molecule at the aqueous interface, accompanied by an increase in the bilayer hydrocarbon thickness.

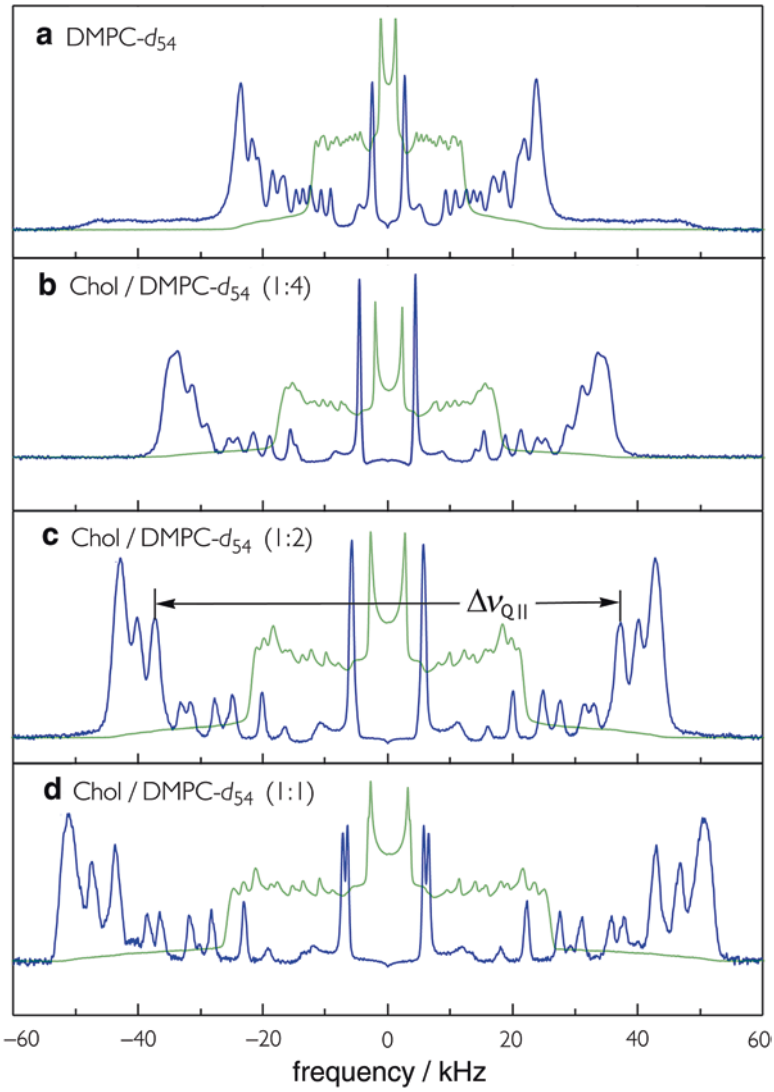

Fig. 2 Solid-state ^{2}H NMR spectra demonstrate the reduction in conformational degrees of freedom for the acyl chain orientation due to cholesterol: (**a**) DMPC-d_{54} in the liquid-disordered (l_d) phase, and (**b**–**d**) DMPC-d_{54} containing various mole fractions of cholesterol in the liquid-ordered (l_o) phase. Data were acquired at a magnetic field strength of 11.7 T (76.8 MHz) at $T = 44$ °C. Powder-type spectra (green) of randomly oriented multilamellar dispersions were numerically inverted (de-Paked) to yield sub-spectra corresponding to the $\theta = 0°$ orientation (blue). Note that a distribution of residual quadrupolar couplings (RQCs) corresponds to the various C^2H_2 and C^2H_3 groups with a progressive increase due to cholesterol. Data are taken from [112]

We can now introduce simplifying precepts from statistical mechanics to further explain the solid-state NMR lineshapes in terms of membrane structural dynamics. For detailed explanations and applications of the statistical mean-torque theory, the interested reader is referred to the literature [30, 65, 70, 73, 138]. The microscopic observables from ^{2}H NMR spectroscopy can then be related to the nano- or microstructure of the membrane lipid assembly. Structural quantities of interest for the lamellar state correspond to the mean interfacial area $\langle A \rangle$, together with the average thickness D_C of the bilayer hydrocarbon region, and the mean aqueous distance separating the lamellae [28, 128, 139–142]. Clearly, the area per lipid molecule plays an important role in molecular dynamics (MD) simulations of lipid membranes [71, 124, 142–148]. The various nanostructures are the result of a balance of forces acting at the level of the polar head groups and hydrocarbon chains [5, 13, 16, 138, 149, 150]. Notably, the deformation of a membrane film away from the equilibrium state is characterized by four material constants: (1) the surface tension γ (which is zero for a membrane bilayer at equilibrium), (2) the area expansion modulus K_A or alternatively the lateral compressibility $C_A \equiv 1/K_A$, (3) the bending rigidity K_C, and (4) the monolayer spontaneous H_0 curvature. The above structural quantities are fundamental to the forces governing the nano- and microstructures of assemblies of membrane lipids and amphiphiles. Representative applications of solid-state ^{2}H NMR spectroscopy to lipid membranes include studies of the influences of cholesterol [151–153] as well as acyl chain polyunsaturation [36, 67, 143, 150, 154–158].

2.2 *Temperature–Composition Phase Diagram of Lipid/Sterol Mixtures*

Lipid-lipid interactions have been investigated for a variety of systems and are important determinants of membrane organization. The lipid composition of the outer leaflet of a typical mammalian plasma membrane mainly comprises sphingomyelin (SM), cholesterol, and unsaturated phosphatidylcholine (PC) [59, 159]. Preferential association of SM and cholesterol has been observed in various membrane environments including enrichment in detergent-resistant membranes [53, 160]; formation of ordered phases in three-component giant unilamellar vesicles [64]; and the direct observation of small domains in the membranes of living cells [161]. Despite the research efforts by many groups into lipid-cholesterol interactions, however, important questions remain concerning the role of cholesterol and other sterols in forming the tightly packed liquid-ordered (l_o) phase. For instance, liquid-disordered (l_d) and (l_o)phases coexist in 1,2-dipalmitoyl-*sn*-glycero-3-phosphocholine (DPPC)/sterol model membranes [75, 162]. Still, the two phases remain submicroscopic in size. Because their small size makes these dynamic domains invisible by most imaging techniques, it has been postulated that l_d/l_o phase coexistence is absent in DPPC/cholesterol model membranes. An alternative explanation

for membrane heterogeneity invokes lipid compositional fluctuations due to proximity to a critical point [126, 163, 164]. Complicating matters further in biological membranes is the asymmetric distribution of lipid molecules between the inner and outer leaflets [165]. In this regard, theoretical descriptions of phospholipid/sterol interactions are extensive [74, 166–170]. The original PC/sterol condensed complex model [166] has been modified to predict phase coexistence in DPPC/cholesterol model membranes above the main transition temperature [171] as well as DPPC phase diagrams with ergosterol [172] and lanosterol [173]. Research in this area remains very active as molecular simulations improve, and experimental input parameters become more accurate [174].

Using solid-state ^{2}H NMR spectroscopy, influences of cholesterol on both the lipid head groups [151] and the acyl chains [152] have been extensively investigated. Cholesterol is located beneath the polar head groups, where it can interact strongly with the acyl chains and act as a spacer molecule, as first suggested [151] in terms of an umbrella-like model. Influences of the acyl chain ordering and dynamics are further discussed below. Previous NMR spectra of DPPC gave the first detailed phase diagram of this cholesterol/lipid mixture [74, 75] and entailed acquiring solid-state ^{2}H NMR spectra for temperatures from 25 to 70 °C and cholesterol concentrations from 0 to 30%. Recently, the binary cholesterol/DPPC phase diagram has been confirmed and extended with 1-palmitoyl-2-perdeuteriopalmitoyl-*sn*-glycero-3-phosphocholine (DPPC-d_{31})/cholesterol membranes [175]. Analogous experiments have been conducted for DPPC-d_{62} using ergosterol [162] and lanosterol [173] as well as N-perdeuteriopalmitoyl-D-erythro-sphingosylphosphorylcholine (PSM-d_{31}). These comparative studies allow insightful comparisons to be made for data obtained using palmitoyl chains with similar conformations. Partial phase diagrams for multilamellar dispersions of *sn*-2 palmitoyl chain-perdeuterated DPPC-d_{31}/cholesterol and for N-linked palmitoyl chain-perdeuterated PSM-d_{31}/cholesterol mixtures have been constructed solely from ^{2}H NMR measurements. Examples of the phase diagrams for the DPPC-d_{31}/cholesterol and PSM-d_{31}/cholesterol multilamellar dispersions obtained from the ^{2}H NMR spectral analysis for various temperatures and cholesterol compositions are shown in Fig. 3. The phase diagrams are very similar and exhibit solid-ordered (s_o) + (l_o) and l_d + l_o coexistence regions with a clear three-phase line separating them [75, 175]. Three regions of two-phase coexistence and a three-phase line are identified in DPPC-d_{31}/cholesterol multilamellar dispersions, as well as in the PSM-d_{31}/cholesterol multilamellar dispersions, thus confirming the basic features of the phase diagram [75]. Narrowing of the l_d + l_o coexistence region at high temperature implies a critical point that corresponds to a cholesterol concentration between ~25 and 30 mol%.

Notably, macroscopic (micron-sized) coexistence of l_d and l_o phases is not observed with solid-state ^{2}H NMR spectroscopy. Instead, spectral line broadening in the l_d + l_o coexistence region points to intermediate exchange of lipids between the two types of domains. The length scales associated with the domains are estimated to be 75–150 nm for DPPC-d_{31}/cholesterol and PSM-d_{31}/cholesterol model membrane mixtures [175]. Distances have been estimated between l_d/l_o domain interfaces in DPPC/cholesterol and PSM/cholesterol multilamellar dispersions to be

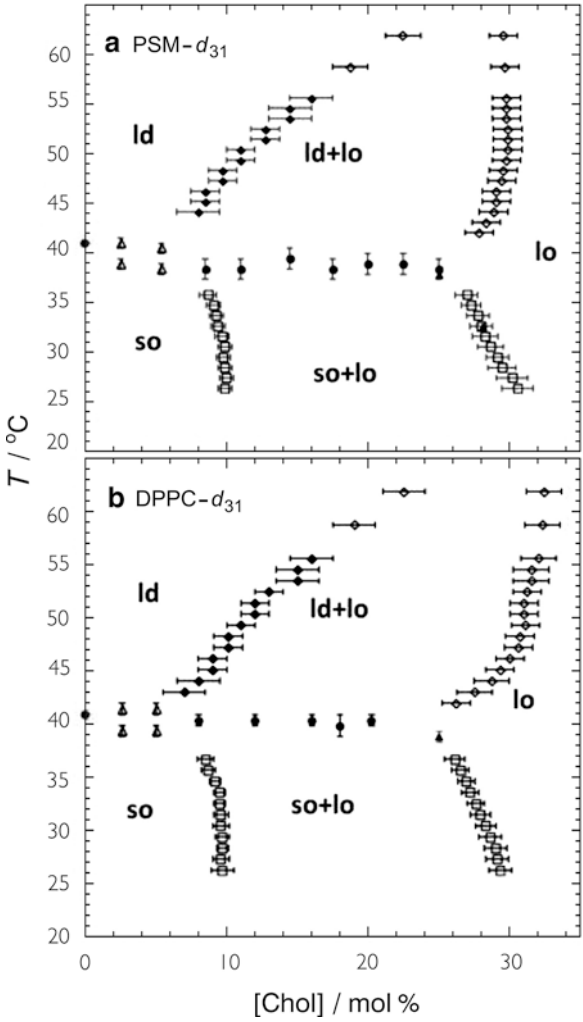

Fig. 3 Partial phase diagrams of: (**a**) PSM-d_{31}/cholesterol and (**b**) DPPC-d_{31}/cholesterol membranes obtained from solid-state ^{2}H NMR spectroscopy. Symbols denote (filled circles) the midpoint of the transition obtained from the de-Paked ^{2}H NMR spectra as a function of temperature; the onset or end of the transition as obtained (open triangles) by inspection of the temperature-dependent spectra, (open squares) from spectral subtractions, (open diamonds) from first-moment M_1 curves, or (filled diamonds) by inspection of the de-Paked spectra against cholesterol concentration; and lastly (filled triangles) the onset of the transition in the first-moment $M_1(T)$ curves. Data are for multilamellar dispersions having cholesterol concentrations of 25 or 28.1 mol% in (**a**) PSM-d_{31}/cholesterol bilayers and 25 mol% in (**b**) DPPC-d_{31}/cholesterol bilayers. Figure modified from [175]

~80 nm. The sizes are on the order of the dimensions of putative rafts in cellular membranes [165]. Hence, if rafts exist in cell membranes, they will be strongly governed by lipid/lipid interactions. The high cholesterol concentration found in many plasma membranes suggests that their preferred physical organization is most likely similar to the l_o phase. With the availability of a detailed picture of the DPPC/cholesterol and PSM/cholesterol binary systems in hand, future ^{2}H NMR studies of ternary raft-like systems [65, 113] can be then conducted to gain added insight into the behavior of lipid rafts in cellular plasma membranes.

2.3 Separated Local-Field ^{13}C NMR Spectroscopy: ^{13}C–^{1}H Dipolar Couplings Allow Calculations of Lipid Bilayer Structure

Lipid membrane systems clearly can benefit from precise structural characterization using solid-state NMR methods. As explained in the previous section, solid-state ^{2}H NMR spectroscopy is prominent among these methods. However, such applications are foreshadowed by the need for ^{2}H-isotope labeling involving synthetic organic chemistry [154, 176]. By the introduction of dipolar-recoupling methods, it is possible to extend the approaches originally developed with regard to solid-state ^{2}H NMR spectroscopy to other classes of biologically relevant lipids, as they occur in a membrane environment. In this regard, separated local-field (SLF) ^{13}C NMR spectroscopy [70, 73, 115, 177, 178] at natural abundance expands the range of applications of solid-state NMR spectroscopy in membrane biophysics. For example, sphingolipids and other natural lipids may be investigated, together with their interactions with cholesterol in raft-like lipid mixtures and with membrane proteins. Additional applications of natural abundance ^{13}C NMR methods to polyunsaturated lipid bilayers [178, 179] have been described. In these examples and others, we are interested in how the molecular properties of membrane lipids explain their biological functions within the broad context of structural biophysics [5, 6, 18, 180].

In what are called separated local-field (SLF) experiments, typically measurements of the direct ^{13}C–^{1}H dipolar couplings are carried out involving liquid-crystalline systems, such as lipid bilayers at natural isotopic abundance. Through-space direct ^{13}C–^{1}H dipolar interactions report on the orientations of the individual ^{13}C–^{1}H bonds with respect to the bilayer normal, and are mathematically isomorphous to the C–^{2}H bond order parameters, measured in solid-state ^{2}H NMR spectroscopy. Various SLF methods include for example dipolar-recoupling methods [70, 73, 106, 115, 177, 181], switched-angle spinning, and off-magic-angle spinning experiments [182]. Segmental order parameters can be unambiguously determined by SLF methods, and hence it is a useful technique for lipid structural studies. In lipid systems, correspondingly the segmental order parameters are defined as:

$$S_{CH} = \frac{1}{2}\left\langle 3\cos^2 \beta_{CH} - 1 \right\rangle \tag{7}$$

where β_{CH} is the instantaneous angle between the ^{13}C–^{1}H bond direction and the bilayer normal. Based on the geometrical considerations, the S_{CH} order parameters for a polymethylene chain are negative. Note that here we refer to the absolute order parameters $|S_{CH}|$, which are calculated from the relation:

$$\left|S_{CH}\right| = \frac{\left|\Delta\nu_D\right|}{\chi_D \chi_P}. \tag{8}$$

In the above formula, $\chi_D = \left(-\mu_0 \gamma_C \gamma_H / 4\pi^2\right)\left\langle r_{CH}^{-3} \right\rangle$ is the dipolar coupling constant (40.783 kHz corresponding to $b_{CH}/2\pi$ = 20.392 kHz for an aliphatic ^{13}C–^{1}H bond), χ_P = 0.393 is the pulse sequence scaling factor [73, 177], and $\Delta\nu_D$ is the measured residual dipolar coupling (RDC) evaluated at the $\theta = 90°$ orientation of the lineshape (Pake powder pattern). An illustration of the results obtained for mixtures of lipids and cholesterol using the dipolar recoupling with shape and scaling preservation (DROSS) experiment is shown in Fig. 4 [73]. The solid-state NMR spectra show well-resolved ^{13}C chemical shifts on the horizontal axis and the site-specific ^{1}H–^{13}C dipolar couplings on the vertical axis. A representative INEPT ^{13}C NMR spectrum showing highly resolved ^{13}C chemical shift resonances for POPC lipid and cholesterol is provided in Fig. 5 [73], which is indicative of the applicability of separated local-field NMR experiments for obtaining the site-specific information about lipid bilayers and lipid mixtures.

3 Molecular Distributions of Lipids are Obtained Using Solid-State ^{2}H NMR Spectral Lineshapes

The solid-state ^{2}H NMR spectrum for 1,2-diperdeuteriomyristoyl-*sn*-glycero-3-phosphocholine (DMPC-d_{54}) at 30 °C shown in Fig. 2a is illustrative of applications to phospholipids with perdeuterated chains in the physiologically relevant, liquid-crystalline state [111, 127]. Because the sample consists of bilayers randomly oriented in the aqueous medium relative to the direction of the magnetic field, the spectrum is a powder-type pattern that is a superposition of signals from the lamellae at all orientations. At each angle, the signal consists of doublets from the chain methyl and methylene positions along the perdeuterated chains [183]. The resulting spectrum has well-defined edges at ~±15 kHz due to a roughly constant order for the acyl methylene segments nearest to the head group of the lipid molecule. Individual peaks within the spectrum arise from less ordered methylene groups in the lower portion of the chains, and the highly disordered terminal methyl group produces the central pair of peaks [128]. From the distribution of the RQCs, structural quantities such as mean area per lipid $\langle A \rangle$ and volumetric bilayer thickness D_C

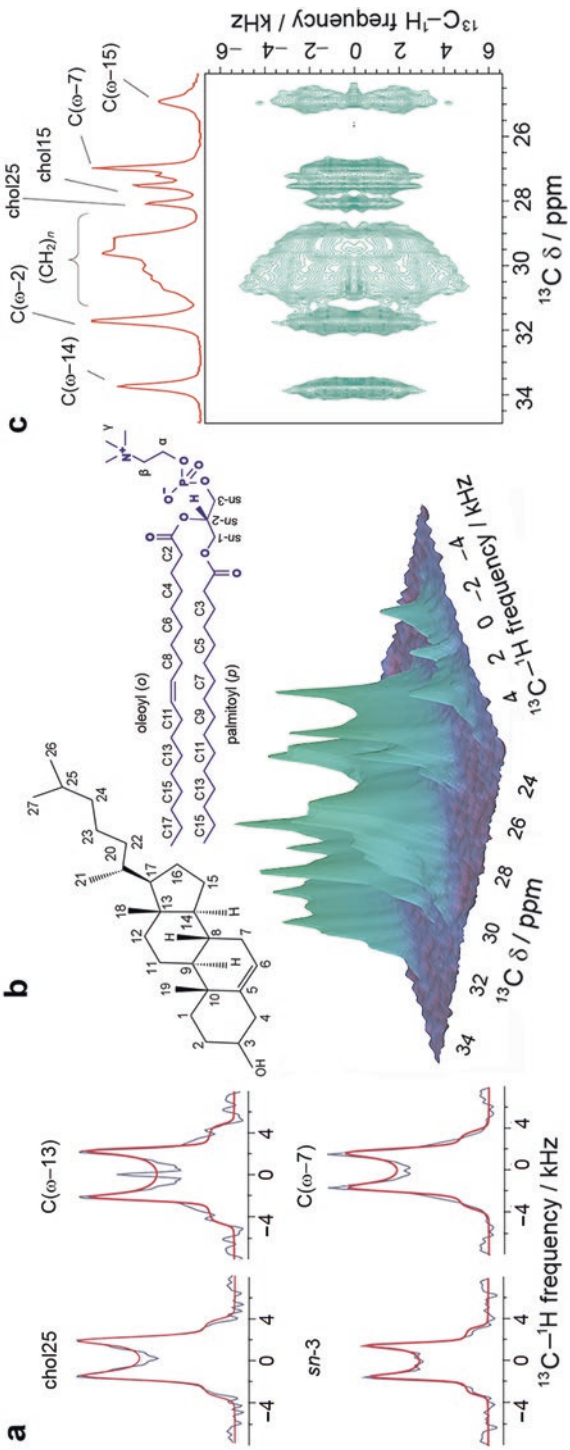

Fig. 4 Site-specific ^{13}C–^{1}H residual dipolar couplings (RDCs) are measured using two-dimensional separated local-field ^{13}C NMR (DROSS) spectrum for POPC/cholesterol (1:1) binary mixture at $T = 30$ °C. (**a**) Selected recoupled powder patterns, showing experimental (gray) and simulated (red) lineshapes. (**b**) Oblique view of aliphatic fingerprint region of the DROSS spectrum of binary system POPC/cholesterol. (**c**) The 2D plane of the spectrum shown in (**b**). The ^{13}C isotropic chemical shift (δ) spectrum is on the horizontal axis (red). The peak separation of the Pake doublet yields the site-specific ^{13}C–^{1}H dipolar couplings along the vertical axis. Figure modified from [73]

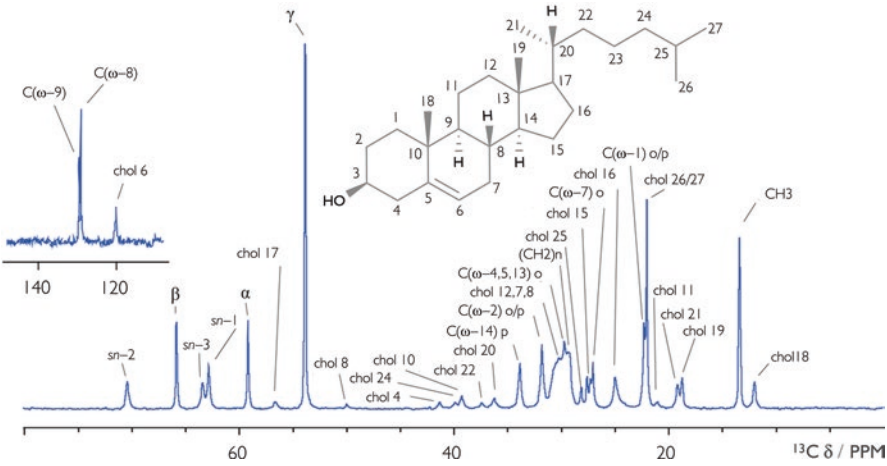

Fig. 5 Experimental INEPT ^{13}C NMR spectrum of the unsaturated lipid 1-palmitoyl-2-oleoyl-*sn*-glycero-3-phosphocholine (POPC) in the presence of 33% cholesterol (chol) at 30 °C. The INEPT experiment is used as part of the separated local-field experiment DROSS. Several highly resolved ^{13}C chemical shifts for POPC and cholesterol show the applicability of separated local-field NMR experiments for obtaining site-specific information on the lipid/cholesterol mixtures. Data obtained from [73]

are readily derived by a mean-torque (MT) model, and can be related to the corresponding material constants or elastic moduli [28, 30, 138]. The significant increase in the observed RQCs upon addition of cholesterol to DMPC bilayers is also shown in a series of spectra from Fig. 2b–d.

3.1 Bilayers Containing Cholesterol Enable Testing of Theories for Dynamical Structures of Membrane Assemblies

In general, lipid bilayers containing cholesterol allow an excellent model for testing theories for the configurational ordering and structural dynamics of liquid-crystalline membranes [30]. As we can see in Fig. 6, for the DMPC-d_{54} bilayer, both in the absence and presence of cholesterol, a well-defined profile of the segmental order parameters $S_{CD}^{(i)}$ versus the acyl segment position (i) is evident. An approximate order parameter plateau occurs over the middle part of the chains, followed by a progressive decrease, which manifests the end effects within the bilayer central hydrocarbon core (Fig. 6). In addition, due to the orientation of the glycerol backbone nearly perpendicular to the membrane surface, the *sn*-1 and *sn*-2 acyl chains are inequivalent [29, 129, 132]. The initial chain geometry leads to smaller order parameters for the beginning of the *sn*-2 chain [143, 184]. Beyond the first few segments, the order parameters of the *sn*-2 chain become larger than those of the *sn*-1

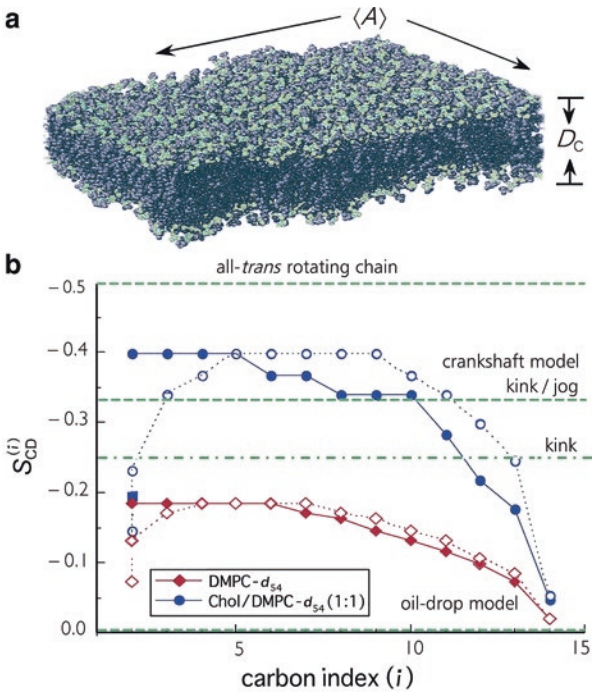

Fig. 6 Comparison of theoretical and solid-state ^{2}H NMR spectroscopy results for the configurational ordering and structural dynamics of liquid-crystalline membranes. The bilayer dimensions correspond to the interfacial membrane area per lipid $\langle A \rangle$ and volumetric thickness D_C. Structural parameters are calculated from the acyl chain volume V_C and moments $\langle \cos \beta \rangle$ and $\langle \cos^2 \beta \rangle$ obtained from the order parameter plateau, where β is the angle between the virtual bond connecting two neighboring carbons of the *i*th segment and bilayer normal [138]. Profiles of segmental order parameters $S_{CD}^{(i)}$ as a function of acyl chain position (i) for DMPC-d_{54} and DMPC-d_{54}/cholesterol (1:1) are shown at $T = 44$ °C [111]. Filled and open symbols refer to inequivalent *sn*-1 and *sn*-2 acyl chains, respectively. Reference order parameters are indicated for limiting cases of an oil-drop model with $S_{CD} = 0$, a crankshaft model having $S_{CD} = -1/3$, and an all-*trans* rotating chain with $S_{CD} = -1/2$. Data are taken from [153]

chain [154]. Smaller statistical fluctuations are associated with greater travel (flux) of the *sn*-2 chain to compensate for the initial position closer to the aqueous interface. The order profile clearly suggests that variations in the degree of acyl chain entanglement occur as a function of depth within the bilayer hydrocarbon region. As a result, it is unlikely that the phospholipids move individually within the bilayer, even in the presence of cholesterol [153, 185, 186].

The approach of using a model membrane, comprising a lipid that forms a fluid bilayer together with a lipid known to form a more ordered bilayer, as well as cholesterol in varying amounts, is probably most accessible as a mimic of biomembranes with a vast number of components [1, 15]. Interestingly, cholesterol has two different functions in model membrane systems: on the one hand, it increases the hydrophobic mismatch of the lipids at low concentrations and thereby enhances

phase separation. On the other hand, it functions as a mixing agent at high concentrations. Let us consider in greater detail the results in Fig. 6 for the DMPC-d_{54} bilayer, both in the absence and presence of cholesterol. To calibrate our intuition, at this point it might be helpful for readers to consider some simple motional models as heuristic guides or limiting cases. Referring again to Fig. 6, the first example is an all-*trans* rotating polymethylene chain, where Eq. (2) with $\beta_{PD} = 90^{o}$ then yields $S_{CD} = -1/2$ as a reference value. Next, we can consider a crankshaft model involving a polymethylene chain that is saturated with kink configurations *gauche*$^{\pm}$-*trans*-*gauche*$^{\mp}$, leading to $S_{CD} = -1/3$ for comparison. Last, the classical oil-drop model completely neglects tethering of the acyl chains to the aqueous interface, in which case the isotropic motion gives $S_{CD} = 0$ as a limit. One can then compare the experimental order profiles to the above limiting cases as benchmarks.

As we have already seen in Fig. 2, for the DMPC-d_{54}/cholesterol (1:1) binary mixture, in the liquid-ordered (l_o) phase there is a dramatic increase in the RQCs versus the liquid-disordered (l_d) phase of DMPC-d_{54} alone. This is due to a substantial reduction of the degrees of freedom of the flexible phospholipids, coming from the van der Waals interactions with the rigid sterol frame. The corresponding plateau in the order profile, cf. Fig. 6, can be understood in terms of a relatively constant probability of the acyl chain configurations, resulting from their tethering via the polar head groups to the aqueous interface, together with their travel (flux) toward the bilayer interior. For the top part of the acyl chains, the segmental order parameters approach the limiting value of $S_{CD} = -1/2$ when cholesterol is present, as expected for an all-*trans* rotating polymethylene chain [112]. However, there is still an approximate plateau indicating entanglement of the chain ends. Note that in the absence of cholesterol, the additional acyl disorder can arise from internal degrees of freedom of the phospholipids, e.g., due to segmental isomerizations, molecular motions, or collective thermal excitations of the bilayer. These additional degrees of freedom lead to smaller absolute S_{CD} values for the DMPC-d_{54} bilayer. Provided that the disorder of the DMPC-d_{54} bilayer is due mainly to rotational isomerism, then the acyl chains fall somewhere between the limiting crankshaft model with $S_{CD} = -1/3$, and the classical oil-drop model for which $S_{CD} = 0$. For the DMPC-d_{54} bilayer, both in the presence and absence of cholesterol, the acyl chains are more disordered within the hydrocarbon core to fill in the free volume that would otherwise be present due to chain terminations, approaching the classical "oil-drop" limit only in the center of the bilayer.

3.2 Order Parameter Profiles of Binary Mixtures of Cholesterol with Phospholipids and Sphingolipids: Implications for Rafts in Cellular Membranes

In addition to glycerophospholipids, most eukaryotic cells contain sphingolipids and sterols as additional classes of lipids (30–40 mol% cholesterol and 10–20 mol% sphingomyelin). Notably, plasma membranes of animal cells are enriched in cholesterol,

which is metabolically derived from lanosterol by removal of the methyl groups from the α-face of the molecule, raising the question of their evolution and function in the organization of the bilayer. Despite extensive research, whether the well-known ordering effect of cholesterol for sphingomyelin and other saturated glycerophospholipids leads to lateral phase segregation and microdomains remains under discussion, as the situation in vivo is far too complex to be exactly determined. However, the structural properties and phase-transition temperatures of sphingomyelins near body temperature (37 °C) suggest that they may play an important role in the formation of specialized domains in membranes, such as lipid rafts [47, 55, 69, 187].

Various studies have been reported on the comparison of order parameter profiles for sphingolipids and phospholipids, and their binary and tertiary mixtures with cholesterol [65, 73, 113, 152, 153]. Results have been obtained from solid-state ^{2}H NMR lineshapes of both POPC-d_{31} and PSM-d_{31} in a complementary way in the corresponding ternary systems. Addition of cholesterol at 20 mol% has been shown to have a major impact on the spectra of PSM-d_{31} in ternary mixtures with POPC (1:1). The range of phase coexistence is increased by the addition of POPC, thereby resisting the formation of the l_d phase from the l_o phase. By contrast, addition of PSM shows an increased ordering effect on the palmitoyl chain in POPC relative to the PSM-free POPC-d_{31}/cholesterol mixture. Analysis of solid-state ^{2}H NMR data using a first-order mean-torque model [65, 138] has uncovered interesting insights into the effect of cholesterol on the lateral organization of lipid-cholesterol mixtures. As described by Bartels et al. [65], the addition of cholesterol initially drives the phase separation (l_d–l_o) by inducing greater lateral order in sphingomyelin than in POPC lipids. However, at 20 mol% cholesterol, discrete components due to POPC-d_{31} and PSM-d_{31} phase separations are observed. At physiological temperature, the lipids in the ternary mixture (1:1 PSM/POPC with 20 mol% cholesterol) show distinct structural parameters (bilayer thickness and area per lipid). Structural parameters of POPC are highly temperature dependent, whereas sphingomyelin shows resistance to thermally driven structural deformation, and stronger affinity of cholesterol that can drive the formation of membrane domains. In mixtures with high amounts of cholesterol (33 mol%), saturation of the ordering effect for PSM seems to facilitate ideal mixing of the components, and hence similar results are observed. These observations naturally bring the intuition that the phase separation is driven by hydrophobic mismatch of the acyl chains of the various lipids, e.g., it is assumed the thickness difference is induced by unequal sterol partitioning into the two phases.

Another study using solid-state ^{13}C NMR spectroscopy [73] has shown that the cholesterol-mediated structural perturbations are less pronounced for egg-yolk sphingomyelin (EYSM) than for POPC. In Fig. 7, the order parameter profiles derived using separated local-field (SLF) ^{13}C NMR spectroscopy for EYSM and POPC bilayers are shown. The influence of cholesterol for the l_o phase of POPC and EYSM is clearly distinguishable. The higher-order parameter values for both the lipid bilayers at various carbon positions are an arresting indication of the l_o phase [6, 65, 92, 106, 111–113, 188–190], due to interaction with cholesterol [191–193]. In addition, the nonequivalence of the segments of the *sn*-1 and *sn*-2 chains [132] is

clearly reflected in the case of the POPC bilayers (Fig. 6a, b). Monounsaturation of the oleoyl chain at the C9 and C10 sites renders the two vinyl ^{13}C–^{1}H positions orientationally nonequivalent, both to each other and to the other saturated chain segments. The terminal methyl groups of the acyl chains exhibit very small residual dipolar couplings (RDC), because of the reorientation and three-fold symmetry of the methyl ^{13}C–^{1}H bonds. The largest couplings of these sites are observed at the C3 position, which may participate in interfacial exchange-type C3–OH hydrogen bonding, and/or C3–OH acceptor and NH donor hydrogen bonding. The large value is suggestive of a glycerol backbone conformation that is stabilized through lipid packing assisted by hydrogen bonding in the l_d phase.

Most striking, upon addition of 50 wt% cholesterol, the increment in segmental order parameters is $\Delta|S_{CH}| \approx 0.25$ for POPC and ≈ 0.12 for EYSM, as indicated in Fig. 7 (comparisons are for the maximum absolute $|S_{CH}|$ values due to the plateau region of the $|S_{CD}|$ profiles). Correspondingly, the increment in the hydrocarbon thickness and condensation of the area per lipid for EYSM is lower than for POPC. Such a remarkable difference indicates that EYSM is in a relatively ordered state in the single-component membrane. The higher acyl segmental order parame-

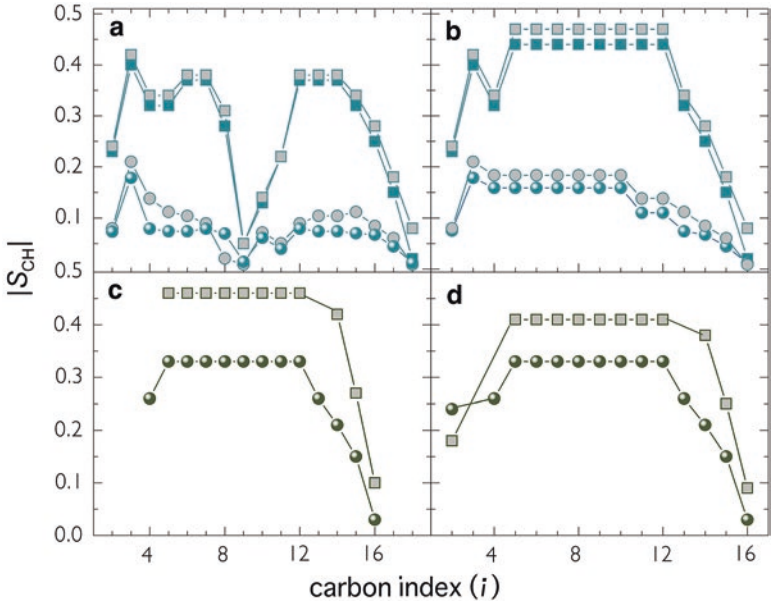

Fig. 7 Segmental order parameter S_{CH} profiles from solid-state ^{13}C NMR spectroscopy (separated local-field) indicate lipid-specific loss of conformational disorder due to cholesterol. Absolute order profiles are plotted for: (**a**) the *sn*-2 oleoyl chain of POPC, (**b**) the *sn*-1 palmitoyl chain of POPC, (**c**) the *sn*-2 sphingosine chain of EYSM, and (**d**) the *sn*-1 palmitoyl chain of EYSM. Circles represent pure lipids and squares represent lipid mixtures with cholesterol (1:1). For POPC, data are shown at two temperatures, $T = 28$ °C (gray-filled symbols) and $T = 48$ °C (solid symbols), and for EYSM at $T = 48$ °C. Note that upon adding cholesterol the absolute S_{CH} order parameters increase more for POPC than in EYSM. Figure adapted from [73]

ters in single-component bilayers at a given temperature, for EYSM relative to POPC, indicate the high propensity of self-association for the hydrophobic moieties of sphingomyelin lipids [55, 69]. Notably, these observations suggest that upon adding cholesterol, the entropic loss is less pronounced for EYSM than for POPC, as discussed in [29]. Mixing of cholesterol is more favorable for sphingolipids compared to phosphatidylcholines, potentially driving the formation of lipid rafts in multicomponent biomembranes [194, 195]. In other words, like dissolves like, as we learn in our introductory chemistry courses.

4 Nuclear Spin Relaxation Reveals Multiscale Dynamics of Membrane Lipids

An important further aspect is that analysis of the nuclear spin relaxation rates yields experimental information about the molecular dynamics that is unobtainable with other biophysical methods [128]. The possible types of motions that occur in lyotropic liquid crystals are: (1) segmental motions due to rotational isomerizations of the flexible surfactant or lipid molecules; (2) slower effective rotations of the entangled molecules; and (3) collective deformations of the bilayer which span a broad range, and can influence interactions involving the assembly [29, 111, 112, 129, 196]. At the high frequencies, bond stretching and bending vibrations are most likely too fast to influence significantly the nuclear spin relaxation, but rather lead to a pre-averaging of the coupling tensor [196, 197]. Identifying the predominant contributions within the various motional regimes, and characterizing their energetic parameters, would reveal the atomistic interactions that lead to bulk material properties based on the current NMR technology [29]. For liquid-crystalline membranes, elastic deformations (modeled as splay, twist, and bend) within the hydrocarbon core are interpreted as collective lipid dynamics on the order of membrane dimensions [127]. It follows that NMR relaxation studies of lipid membranes in the l_o and l_d phases can strongly benefit our understanding of the atomistic lipid–cholesterol interactions, leading to changes in bulk membrane physical properties, with striking biological consequences.

4.1 Fluctuating Molecular Interactions Due to Various Types of Lipid Motions Within the Bilayer Cause the Nuclear Spin Relaxation

The process of NMR relaxation is due to fluctuations of the coupling Hamiltonian, on account of the various possible motions of the lipid molecules within the bilayer. According to time-dependent perturbation theory, these fluctuations give rise to transitions between the various adjacent energy levels [136]. In ^{2}H NMR relaxometry of

liquid-crystalline membrane lipids, one is often interested in the spin–lattice (R_{1Z}) relaxation rates. Experimental R_{1Z} relaxation rate measurements involve perturbation of the magnetization away from the equilibrium value, and then following the attainment of equilibrium by observing the magnetization recovery as a function of time. The observable relaxation rates are related to the spectral densities of motion in the laboratory frame by:

$$R_{1Z} = \frac{3}{4}\pi^2 \chi_Q^2 \left[J_1(\omega_0) + 4J_2(2\omega_0) \right]. \tag{9}$$

In the above expression, R_{1Z} is the spin–lattice (longitudinal) relaxation rate, and $J_m(\omega_0)$ denotes the irreducible spectral densities of motion, where $m = 1$, 2, and ω_0 is the deuteron Larmor frequency. The spectral densities $J_m(\omega_0)$ describe the power spectrum of the motions as a function of frequency ω_0 in terms of fluctuations of the Wigner rotation matrix elements for transformation of the coupling (EFG) tensor from its principal axis system to the laboratory frame. They are the Fourier transform partners of the orientational correlation functions $G_m(t)$ which depend on time, and characterize the C–^{2}H bond fluctuations.

4.2 Generalized Model-Free Aspects of the Nuclear Spin Relaxation of Membrane Lipid Bilayers

Here, we give a brief introduction to the model-free interpretation of the relaxation rates for general readers, while dealing with actual lipid relaxation data. For a more complete description of generalized model-free (GMF) analysis, readers are referred to the review by Xu et al. [136]. Contributions to the nuclear spin relaxation from motions with different characteristic mean-squared amplitudes and timescales are possible in terms of a hierarchical energy landscape [185]. They include: (1) the static coupling tensor that is modulated by rapid local segmental motions, such as *trans-gauche* isomerizations of the hydrocarbon chains of the lipid or surfactant molecules; and (2) the residual coupling tensor (leftover from the fast motions) that is further modulated by slower motions. The slower motions in principle might include whole-molecule motions of the flexible phospholipids, or alternatively collective thermal excitations involving the various lipid molecules [146, 198]. Clearly, the segmental order parameters depend only on the amplitudes of the C–^{2}H bond fluctuations. On the other hand, the relaxation rates depend on both the orientational amplitudes and the rates of the C–^{2}H bond fluctuations. According to the GMF approach of relaxation rate analysis [136, 197, 199], a simple linear dependence of the R_{1Z} rates on the squared segmental order parameters (S_{CD}^2) (square-law) along the chain would result (Fig. 8). In the limit of short-wavelength excitations, on the order of the bilayer thickness and less, the spectral density reads [200]:

$$J_m(\omega) = \frac{5}{2} S_{CD}^2 D \omega^{-(2-d/2)} \left[\left| D_{-1m}^{(2)}(\beta_{DL}) \right|^2 + \left| D_{1m}^{(2)}(\beta_{DL}) \right|^2 \right]. \tag{10}$$

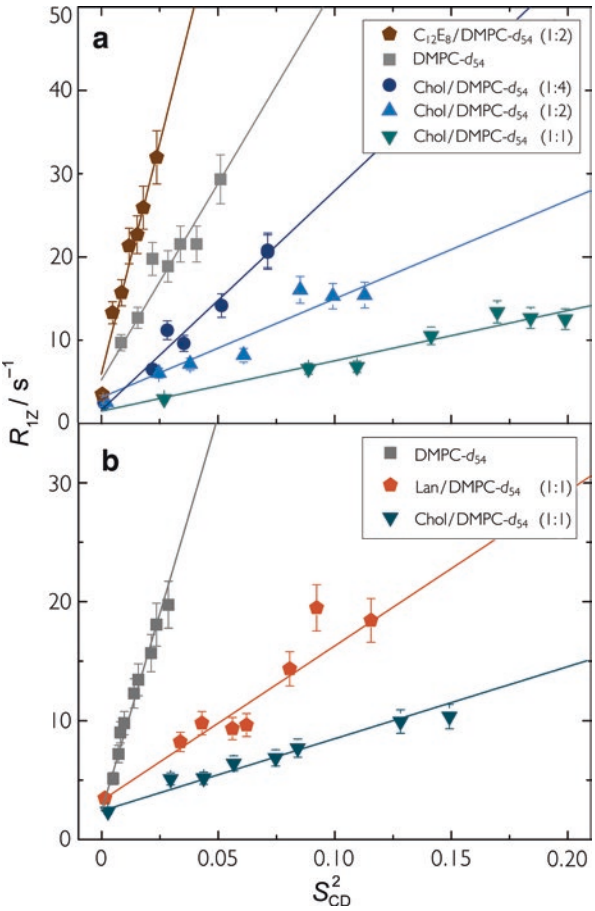

Fig. 8 Solid-state ^{2}H NMR relaxation at 76.8 MHz (11.8 T) shows emergence of membrane elastic fluctuations and their suppression by sterols. Striking differences are uncovered in membrane elastic fluctuations from cholesterol versus lanosterol at the atomistic level. (**a**) Dependence of spin–lattice relaxation rates $R_{1Z}^{(i)}$ on squared order parameters $S_{CD}^{(i)}$ for resolved ^{2}H NMR splittings of DMPC-d_{54} showing influences of cholesterol in the liquid-ordered (l_o) phase at T = 44 °C. The presence of cholesterol leads to a large decrease in the square-law slopes, corresponding to a progressive reduction in bilayer elasticity. An opposite increase is seen for bilayers containing $C_{12}E_8$ nonionic detergent at T = 42 °C. Data are taken from [129]. (**b**) Dependence of spin–lattice relaxation rates $R_{1Z}^{(i)}$ on squared order parameters $S_{CD}^{(i)}$ in liquid-ordered phase (l_o) for resolved ^{2}H NMR splittings of DMPC-d_{54} showing influences of lanosterol and cholesterol at T = 55 °C. Note that the decrease in the square-law slopes is consistent with a gradual reduction in bilayer elasticity on going from lanosterol to cholesterol. Data are taken from [112]

Here, ω is the angular frequency, D is the viscoelastic constant, d is the dimensionality, and $D^{(2)}$ indicates the second-rank Wigner rotation matrix [137]. The irreducible spectral densities $J_m(\omega)$ depend on the square of the observed S_{CD} order

parameters, and the slope of the square-law plot is inversely related to the softness of the membrane. For 3D quasielastic fluctuations, the viscoelastic constant is given by $D = 3k_{\mathrm{B}}T\sqrt{\eta}\,/\,5\pi\sqrt{2K^3}S_{\mathrm{s}}^2$, where a single elastic constant K is assumed, in which η is the corresponding viscosity coefficient, S_s is the order parameter for the relatively slow motions, and other symbols have their usual meanings. No distinction is made between splay, twist, and bend deformations. In addition to the bending modulus κ, the compression modulus K_B may come into play [141].

4.3 Nuclear Spin Relaxation of Lipid Membranes in the Liquid-Ordered Phases Reveals Atomistic Lipid–Cholesterol Interactions and Bulk Membrane Physical Properties

In the example presented here, a solid-state ^{2}H NMR relaxation study of effect of cholesterol on lipid bilayers shows that a square-law functional dependence of the R_{1Z} rates versus the order parameters S_{CD} is evident along the entire acyl chain for the multilamellar dispersions of DMPC-d_{54}/cholesterol bilayers (Fig. 8a) [111]. This dependence on the motional amplitudes signifies relatively slow bilayer motions that modulate the residual coupling tensors leftover from faster segmental motions (Fermi's golden rule). Given a simple composite membrane deformation model [196, 201], the R_{1Z} rates are due to a broad spectrum of 3D collective bilayer excitations, with effective rotations of the lipids. Transverse ^{2}H NMR spin relaxation studies also provide evidence for 2D collective motions of the membrane film, albeit at lower frequencies [202–205]. By contrast, local *trans-gauche* isomerizations along the chains modulate the same *static* NMR coupling tensor, and do not yield such a square-law. With regard to splay deformations, the so-called bending rigidity is $\kappa \approx Kt$, where $t = 2D_{\mathrm{C}}$ is the bilayer thickness, giving a $\kappa^{-3/2}$ dependence of the R_{1Z} rates [127]. Moreover, 3D director fluctuations ($d = 3$) yield a $\omega^{-1/2}$ frequency dispersion as a characteristic signature [185, 206]. In this case, the reduction in the square-law slope, cf. Fig. 8a, b, reflects an increase in κ and/or S_{s} due to short-range cholesterol–phospholipid interactions. One should also note that at the molecular level, a dynamical protrusion of cholesterol across the midplane, i.e., between the apposed monolayers, is suggested by quasielastic neutron scattering studies [27, 207]. Indeed, the square-law functional dependence as first discussed [185] is a model-free correlation among the experimental observables, and it does not rest on any specific molecular interpretation. For the longitudinal relaxation rates of liquid-crystalline lipid membranes, the above analysis is expected to be generally applicable.

4.4 The Progressive Increase in Bilayer Rigidity from Lanosterol to Cholesterol Parallels the Metabolic Pathway of Sterol Biogenesis

Influences of cholesterol on the physical properties of DMPC bilayers have also been compared to its metabolic precursor lanosterol in a related study [112] (Fig. 8b). Notably, cholesterol is a two-faced molecule—the α-face is smooth and the β-face is molecularly rough due to the methyl substituents. Even so, lanosterol is methylated on both the α-face and the β-face (Fig. 1), and it presents a more balanced countenance to the phospholipids [208]. In terms of biomolecular NMR spectroscopy, it has been observed that the slope of the square-law plot is greater for lanosterol than for cholesterol, consistent with the bilayer stiffness being less for lanosterol versus its metabolic product cholesterol [25, 112, 209]. Again, it is found that the site-specific analysis of the solid-state NMR results based on atomistic observables matches the results for the macroscopic bilayer elasticity [207, 210] (Fig. 9). The more molecularly smooth van der Waals surface of the α-face of cholesterol [92, 193, 211, 212] enables a large increase in bilayer rigidity and stabilizes the liquid-ordered phase to an even greater degree than lanosterol. Figure 9a illustrates the comparison of the bending rigidity (modulus) (κ) for the DMPC bilayers using deuterium NMR relaxometry and thermal shape fluctuation data. The progressive increase in the bilayer rigidity on going from lanosterol to cholesterol (Fig. 9b) parallels the metabolic pathway of sterol biogenesis [162, 173, 213–217], and may be related to the optimization or evolution of the biophysical properties of cholesterol. In a similar study, the effect of several sterols on the lipid order and bilayer rigidity has been investigated for macroscopically aligned bilayers of DMPC or DPPC using ^{2}H NMR spectra and spin–lattice relaxation rates [25]. The bending modulus of the bilayers was calculated from plots of the relaxation rates versus the square of the order parameter. Clear differences were obtained in the efficiency of the sterols to increase the stiffness of the bilayers. These differences are correlated to the ability of the sterols to induce the liquid-ordered phase in binary as well as in ternary systems.

5 Biophysical Conclusions and Outlook

Solid-state NMR methods offer excellent experimental techniques in medicine and biology. They uniquely probe the physical properties of lipid membranes and provide information complementary to other spectroscopic methods. Interestingly, owing to their physiological liquid-crystalline nature, membrane elastic deformations together with their multiscale molecular dynamics clearly fall in the solid-state ^{2}H NMR time- and length scales. The membrane stiffening effect upon addition of sterols has been investigated at an atomistically resolved level, showing a direct correspondence with bulk elasticity. Phase separation in bilayers of ternary lipid

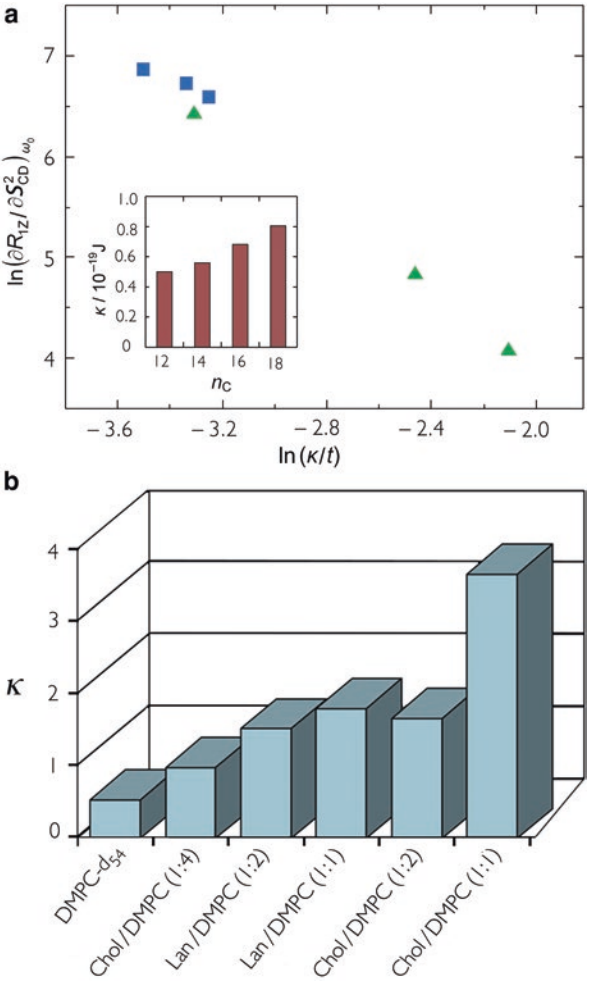

Fig. 9 Bending rigidity of lipid bilayers obtained from solid-state ^{2}H NMR relaxation analysis. (**a**) Comparison of solid-state ^{2}H NMR square-law slopes to bending rigidity κ obtained from thermal shape fluctuation data for lipid vesicles. Results for homologous series of PCs with acyl carbon lengths of n_C = 12, 14, and 16 in the liquid-disordered (l_d) phase at 55.4 MHz (squares); data at 76.8 MHz for DMPC/cholesterol mixtures with X_C = 0, 0.33, and 0.50 in the liquid-ordered (l_o) phase (triangles). The inset shows the values of κ estimated from the ^{2}H NMR model for the homologous series of PCs. Bending rigidity estimates from solid-state ^{2}H NMR are in good agreement with the values obtained from thermal shape fluctuation data. Figure adapted from [111]. (**b**) Comparison of bending rigidities of DMPC lipid bilayers obtained by solid-state ^{2}H NMR relaxation at various compositions of DMPC and cholesterol (Chol/DMPC), and DMPC and lanosterol (Lan/DMPC) mixtures. Significant difference is seen in the influence of cholesterol versus lanosterol on the elastic properties of DMPC membrane bilayers. Data taken from [112]

mixtures occurs mainly due to dissimilar affinities for different cholesterol concentrations. It is likely that configurational entropy plays a major role in the formation of the lipid domains called rafts [73]. It has also been shown in model membranes [20, 46, 47, 218] that formation of such domains entails Gibbs free energies that are lower than those for protein-lipid interactions, which therefore may indicate a role for proteins in domain formation. Further detailed information regarding protein–lipid interactions can contribute to understanding the lateral organization of cellular plasma membranes, and how lipid rafts may be implicated in their functional mechanisms. Moreover, nuclear spin–lattice relaxation studies of fluid lipid bilayers manifest their quasielastic deformation on short length and timescales, on the order of the membrane thickness and less. Interpretation of the atom-specific NMR relaxation data is in broad agreement with molecular dynamics (MD) simulations of flexible surfactant films and lipid membranes [51, 142, 146, 198, 219]. Molecular simulations [219] show that local *trans-gauche* isomerizations are accompanied by concerted isomerizations about multiple bonds in the assembly of lipid acyl chains. The continuum model for NMR relaxation approximates the collective excitations in mathematical closed form, wherein the influences of cholesterol and the membrane thickness correspond to the bilayer bending energy. A key remaining question is how the bilayer softness as studied with NMR relaxation may be significant to lipid–protein interactions in fluid membranes [6, 220–222], where elastic curvature deformation may play an important role.

Acknowledgments This research was supported by the US National Institutes of Health. The authors are grateful to the past and present members of our laboratory for their many outstanding contributions to the research in this chapter.

References

1. van Meer G, Voelker DR, Feigenson GW. Membrane lipids: where they are and how they behave. Nat Rev Mol Cell Biol. 2008;9:112–24.
2. Krause MR, Regen SL. The structural role of cholesterol in cell membranes: from condensed bilayers to lipid rafts. Acc Chem Res. 2014;47:3512–21.
3. Maxfield FR, Tabas I. Role of cholesterol and lipid organization in disease. Nature. 2005; 438:612–21.
4. Yeagle PL. Modulation of membrane function by cholesterol. Biochimie. 1991;73:1303–10.
5. Brown MF. Modulation of rhodopsin function by properties of the membrane bilayer. Chem Phys Lipids. 1994;73:159–80.
6. Brown MF. Curvature forces in membrane lipid-protein interactions. Biochemistry. 2012;51: 9782–95.
7. Brown MF. Soft matter in lipid–protein interactions. Annu Rev Biophys. 2017;46:379–410.
8. Sheng R, Chen Y, Gee HY, Stec E, Melowic HR, Blatner NR, Tun MP, Kim Y, Källberg M, Fujiwara TK, Hong JH, Kim KP, Lu H, Kusumi A, Lee MG, Cho W. Cholesterol modulates cell signaling and protein networking by specifically interacting with PDZ domain-containing scaffold proteins. Nat Commun. 2012;3:1249.
9. Huang P, Nedelcu D, Watanabe M, Jao C, Kim Y, Liu J, Salic A. Cellular cholesterol directly activates smoothened in Hedgehog signaling. Cell. 2016;166:1176–87.

10. Liu S-L, Sheng R, Jung JH, Wang L, Stec E, O'Connor MJ, Song S, Bikkavilli RK, Winn RA, Lee D, Baek K, Ueda K, Levitan I, Kim K-P, Cho W. Orthogonal lipid sensors identify transbilayer asymmetry of plasma membrane cholesterol. Nature Chem Biol. 2016;13:268–74.
11. Molugu TR, Brown MF. Cholesterol-induced suppression of membrane elastic fluctuations at the atomistic level. Chem Phys Lipids. 2016;199:39–51.
12. Arriaga LR, Rodriguez-Garcia R, Moleiro LH, Prevost S, Lopez-Montero I, Hellweg T, Monroy F. Dissipative dynamics of fluid lipid membranes enriched in cholesterol. Adv Colloid Interface Sci. 2017;247:514–20.
13. Seddon JM. Structure of the inverted hexagonal (H_{II}) phase, and non-lamellar phase transitions of lipids. Biochim Biophys Acta. 1990;1031:1–69.
14. Seddon JM, Templer RH, Warrender NA, Huang Z, Cevc G, Marsh D. Phosphatidylcholine-fatty acid membranes: effects of headgroup hydration on the phase behaviour and structural parameters of the gel and inverse hexagonal (H_{II}) phases. Biochim Biophys Acta. 1997;1327:131–47.
15. Feigenson GW. Phase behavior of lipid mixtures. Nature Chem Biol. 2006;2:560–3.
16. Zimmerberg J, Gawrisch K. The physical chemistry of biological membranes. Nature Chem Biol. 2006;2:564–7.
17. Krepkiy D, Mihailescu M, Freites JA, Schow EV, Worcester DL, Gawrisch K, Tobias DJ, White SH, Swartz KJ. Structure and hydration of membranes embedded with voltage-sensing domains. Nature. 2009;462:473–9.
18. Phillips R, Ursell T, Wiggins P, Sens P. Emerging roles for lipids in shaping membrane-protein function. Nature. 2009;459:379–85.
19. Amazon JJ, Feigenson GW. Lattice simulations of phase morphology on lipid bilayers: renormalization, membrane shape, and electrostatic dipole interactions. Phys Rev E. 2014;89:022702.
20. Feigenson GW. Pictures of the substructure of liquid-ordered domains. Biophys J. 2015; 109:854–5.
21. Rheinstädter MC, Ollinger C, Fragneto G, Demmel F, Salditt T. Collective dynamics of lipid membranes studied by inelastic neutron scattering. Phys Rev Lett. 2004;93:108107.
22. Brown MF, Chan SI. Bilayer membranes: deuterium and carbon-13 NMR. eMagRes. 2007:1–15.
23. Tyler AI, Clarke J, Seddon J, Law R. Solid state NMR of lipid model membranes. In: Owen DM, editor. Methods in membrane lipids. New York: Springer; 2015. p. 227–53.
24. Kaiser H-J, Lingwood D, Levental I, Sampaio JL, Kalvodova L, Rajendran L, Simons K. Order of lipid phases in model and plasma membranes. Proc Natl Acad Sci U S A. 2009; 106:16645–50.
25. Orädd G, Shahedi V, Lindblom G. Effect of sterol structure on the bending rigidity of lipid membranes: a ^{2}H NMR transverse relaxation study. Biochim Biophys Acta. 2009;1788:1762–71.
26. Coskun U, Simons K. Cell membranes: the lipid perspective. Structure. 2011;19:1543–8.
27. Kaye MD, Schmalzl K, Nibali VC, Tarek M, Rheinstädter MC. Ethanol enhances collective dynamics of lipid membranes. Phys Rev E. 2011;83(5 Pt 1):050907.
28. Mallikarjunaiah KJ, Leftin A, Kinnun JJ, Justice MJ, Rogozea AL, Petrache HI, Brown MF. Solid-state ^{2}H NMR shows equivalence of dehydration and osmotic pressures in lipid membrane deformation. Biophys J. 2011;100:98–107.
29. Leftin A, Xu X, Brown MF. Phospholipid bilayer membranes: deuterium and carbon-13 NMR spectroscopy. eMagRes. 2014;3:199–214.
30. Kinnun JJ, Mallikarjunaiah KJ, Petrache HI, Brown MF. Elastic deformation and area per lipid of membranes: atomistic view from solid-state deuterium NMR spectroscopy. Biochim Biophys Acta. 2015;1848:246–59.
31. Shaghaghi M, Keyvanloo A, Huang ZH, Szoka FC, Thewalt JL. Constrained versus free cholesterol in DPPC membranes: a comparison of chain ordering ability using deuterium NMR. Langmuir. 2017;33:14405–13.
32. Thewalt JL. Essential insights into lipid membrane organization from essential fatty acids. Biophys J. 2018;114:254–5.

33. Molugu TR, Xu X, Lee S, Mallikarjunaiah KJ, Brown MF. Solid-state ^{2}H NMR studies of water-mediated lipid membrane deformation. In: Webb GA, editor. Modern magnetic resonance. Cham: Springer; 2018. p. 1–27.
34. Soubias O, Teague WE Jr, Hines KG, Gawrisch K. Rhodopsin/lipid hydrophobic matching-rhodopsin oligomerization and function. Biophys J. 2015;108:1125–32.
35. Chawla U, Jiang YJ, Zheng W, Kuang LJ, Perera SMDC, Pitman MC, Brown MF, Liang HJ. A usual G-protein-coupled receptor in unusual membranes. Angew Chem Int Ed. 2016;55:588–92.
36. Teague WE Jr, Soubias O, Petrache H, Fuller N, Hines KG, Rand RP, Gawrisch K. Elastic properties of polyunsaturated phosphatidylethanolamines influence rhodopsin function. Faraday Discuss. 2013;161:383–95.
37. Liang R, Li H, Swanson JMJ, Voth GA. Multiscale simulation reveals a multifaceted mechanism of proton permeation through the influenza A M2 proton channel. Proc Natl Acad Sci U S A. 2014;111:9396–401.
38. Soubias O, Teague WE, Hines KG, Gawrisch K. The role of membrane curvature elastic stress for function of rhodopsin-like G protein-coupled receptors. Biochimie. 2014;107:28–32.
39. Gondré-Lewis MC, Petrache HI, Wassif CA, Harries D, Parsegian A, Porter FD, Loh YP. Abnormal sterols in cholesterol-deficiency diseases cause secretory granule malformation and decreased membrane curvature. J Cell Sci. 2006;119:1876–85.
40. Kumar GA, Jafurulla M, Chattopadhyay A. The membrane as the gatekeeper of infection: cholesterol in host–pathogen interaction. Chem Phys Lipids. 2016;199:179–85.
41. Eriksson JC, Henriksson U. Bridging-cluster model for hydrophobic attraction. Langmuir. 2007;23:10026–33.
42. Goñi FM, Alonso A, Bagatolli LA, Brown RE, Marsh D, Prieto M, Thewalt JL. Phase diagrams of lipid mixtures relevant to the study of membrane rafts. Biochim Biophys Acta. 2008;1781:665–84.
43. Escriba PV, Gonzalez-Ros JM, Goni FM, Kinnunen PKJ, Vigh L, Sanchez-Magraner L, Fernandez AM, Busquets X, Horvath I, Barcelo-Coblijn G. Membranes: a meeting point for lipids, proteins and therapies. J Cell Mol Med. 2008;12:829–75.
44. Armstrong CL, Barrett MA, Hiess A, Salditt T, Katsaras J, Shi A-C, Rheinstädter MC. Effect of cholesterol on the lateral nanoscale dynamics of fluid membranes. Eur Biophys J. 2012; 41:901–13.
45. Armstrong CL, Marquardt D, Dies H, Kučerka N, Yamani Z, Harroun TA, Katsaras J, Shi A-C, Rheinstädter MC. The observation of highly ordered domains in membranes with cholesterol. Plos One. 2013;8:e66162.
46. Ackerman DG, Feigenson GW. Multiscale modeling of four-component lipid mixtures: domain composition, size, alignment, and properties of the phase interface. J Phys Chem B. 2015;119:4240–50.
47. Konyakhina TM, Feigenson GW. Phase diagram of a polyunsaturated lipid mixture: brain sphingomyelin/1-stearoyl-2-docosahexaenoyl-*sn*-glycero-3-phosphocholine/cholesterol. Biochim Biophys Acta. 2016;1858:153–61.
48. Epand RM. Lipid polymorphism and protein-lipid interactions. Biochim Biophys Acta. 1998; 1376:353–68.
49. Epand RM. Cholesterol and the interaction of proteins with membrane domains. Prog Lipid Res. 2006;45:279–94.
50. Scheidt HA, Meyer T, Nikolaus J, Baek DJ, Haralampiev I, Thomas L, Bittman R, Mueller P, Herrmann A, Huster D. Cholesterol's aliphatic side chain modulates membrane properties. Angew Chem Int Ed. 2013;52:12848–51.
51. Sodt AJ, Sandar ML, Gawrisch K, Pastor RW, Lyman E. The molecular structure of the liquid-ordered phase of lipid bilayers. J Am Chem Soc. 2014;136:725–32.
52. Levental I, Veatch SL. The continuing mystery of lipid rafts. J Mol Biol. 2016;428:4749–64.
53. Brown DA, London E. Functions of lipid rafts in biological membranes. Annu Rev Cell Dev Biol. 1998;14:111–36.

54. Golebiewska U, Scarlata S. The effect of membrane domains on the G protein-phospholipase Cβ signaling pathway. Crit Rev Biochem Mol Biol. 2010;45:97–105.
55. Simons K, Gerl MJ. Revitalizing membrane rafts: new tools and insights. Nat Rev Mol Cell Biol. 2010;11:688–99.
56. Simons K, Sampaio JL. Membrane organization and lipid rafts. Cold Spring Harb Perspect Biol. 2011;3:a004697.
57. Surma MA, Klose C, Simons K. Lipid-dependent protein sorting at the trans-Golgi network. Biochim Biophys Acta. 2012;1821:1059–67.
58. Klose C, Surma MA, Simons K. Organellar lipidomics – background and perspectives. Curr Opin Cell Biol. 2013;25:406–13.
59. Song Y, Kenworthy AK, Sanders CR. Cholesterol as a co-solvent and a ligand for membrane proteins. Prot Sci. 2014;23:1–22.
60. Day CA, Kenworthy AK. Functions of cholera toxin B-subunit as a raft cross-linker. Essays Biochem. 2015;57:135–45.
61. Keller SL, McConnell HM. Stripe phases in lipid monolayers near a miscibility critical point. Phys Rev Lett. 1999;82:1602–5.
62. Edidin M. The state of lipid rafts: from model membranes to cells. Annu Rev Biophys Biomol Struct. 2003;32:257–83.
63. Polozov IV, Gawrisch K. Characterization of the liquid-ordered state by proton MAS NMR. Biophys J. 2006;90:2051–61.
64. Veatch SL, Soubias O, Keller SL, Gawrisch K. Critical fluctuations in domain-forming lipid mixtures. Proc Natl Acad Sci U S A. 2007;104:17650–5.
65. Bartels T, Lankalapally RS, Bittman R, Beyer K, Brown MF. Raftlike mixtures of sphingomyelin and cholesterol investigated by solid-state ^{2}H NMR spectroscopy. J Am Chem Soc. 2008;130:14521–32.
66. Korade Z, Kenworthy AK. Lipid rafts, cholesterol, and the brain. Neuropharmacology. 2008;55:1265–73.
67. Wassall SR, Stillwell W. Polyunsaturated fatty acid-cholesterol interactions: domain formation in membranes. Biochim Biophys Acta. 2009;1788:24–32.
68. Camley BA, Brown FLH. Dynamic simulations of multicomponent lipid membranes over long length and time scales. Phys Rev Lett. 2010;105:148102.
69. Lingwood D, Simons K. Lipid rafts as a membrane-organizing principle. Science. 2010; 327:46–50.
70. Leftin A, Job C, Beyer K, Brown MF. Solid-state ^{13}C NMR reveals annealing of raft-like membranes containing cholesterol by the intrinsically disordered protein α-synuclein. J Mol Biol. 2013;425:2973–87.
71. Meinhardt S, Vink RLC, Schmid F. Monolayer curvature stabilizes nanoscale raft domains in mixed lipid bilayers. Proc Natl Acad Sci U S A. 2013;110:4476–81.
72. Quinn PJ. Structure of sphingomyelin bilayers and complexes with cholesterol forming membrane rafts. Langmuir. 2013;29:9447–56.
73. Leftin A, Molugu TR, Job C, Beyer K, Brown MF. Area per lipid and cholesterol interactions in membranes by separated local-field ^{13}C NMR spectroscopy. Biophys J. 2014;107:2274–86.
74. Ipsen JH, Karlström G, Mouritsen OG, Wennerström H, Zuckermann MJ. Phase equilibria in the phosphatidylcholine-cholesterol system. Biochim Biophys Acta. 1987;905:162–72.
75. Vist MR, Davis JH. Phase-equilibria of cholesterol dipalmitoylphosphatidylcholine mixtures: ^{2}H nuclear magnetic-resonance and differential scanning calorimetry. Biochemistry. 1990;29:451–64.
76. Simons K, Ikonen E. How cells handle cholesterol. Science. 2000;290:1721–6.
77. Simons K, Toomre D. Lipid rafts and signal transduction. Nat Rev Mol Cell Biol. 2000;1:31–9.
78. Ge Y, Gao J, Jordan R, Naumann CA. Changes in cholesterol level alter integrin sequestration in raft-mimicking lipid mixtures. Biophys J. 2018;114:158–67.
79. Greenwood AI, Pan J, Mills TT, Nagle JF, Epand RM, Tristram-Nagle S. CRAC motif peptide of the HIV-1 gp41 protein thins SOPC membranes and interacts with cholesterol. Biochim Biophys Acta. 2008;1778:1120–30.

80. Baier CJ, Fantini J, Barrantes FJ. Disclosure of cholesterol recognition motifs in transmembrane domains of the human nicotinic acetylcholine receptor. Sci Rep. 2011;69:1–7.
81. Fantini J, Barrantes FJ. How cholesterol interacts with membrane proteins: an exploration of cholesterol-binding sites including CRAC, CARC, and tilted domains. Front Physiol. 2013;4:1–9.
82. Koufos E, Chang EH, Rasti ES, Krueger E, Brown AC. Use of a cholesterol recognition amino acid consensus peptide to inhibit binding of a bacterial toxin to cholesterol. Biochemistry. 2016;55:4787–97.
83. Jafurulla M, Tiwari S, Chattopadhyay A. Identification of cholesterol recognition amino acid consensus (CRAC) motif in G-protein coupled receptors. Biochim Biophys Res Commun. 2011;404:569–73.
84. Vogel A, Tan K-T, Waldmann H, Feller SE, Brown MF, Huster D. Flexibility of Ras lipid modifications studied by ^{2}H solid-state NMR and molecular dynamics simulations. Biophys J. 2007;93:2697–712.
85. Weise K, Huster D, Kapoor S, Triola G, Waldmann H, Winter R. Gibbs energy determinants of lipoprotein insertion into lipid membranes: the case study of Ras proteins. Faraday Discuss. 2013;161:549–61.
86. Hubbell WL, McConnell HM. Molecular motion in spin-labeled phospholipids and membranes. J Am Chem Soc. 1971;93:314–26.
87. Semer R, Gelerinter E. Spin label study of the effects of sterols on egg lecithin bilayers. Chem Phys Lipids. 1979;23:201–11.
88. Delmelle M, Butler KW, Smith ICP. Saturation transfer electron-spin resonance spectroscopy as a probe of anisotropic motion in model membrane systems. Biochemistry. 1980;19:698–704.
89. Manukovsky N, Sanders E, Matalon E, Wolf SG, Goldfarb D. Membrane curvature and cholesterol effects on lipids packing and spin-labelled lipids conformational distributions. Mol Phys. 2013;111:2887–96.
90. Williams JA, Wassall CD, Kemple MD, Wassall SR. An electron paramagnetic resonance method for measuring the affinity of a spin-labeled analog of cholesterol for phospholipids. J Membr Biol. 2013;246:689–96.
91. Cheng C-Y, Olijve LLC, Kausik R, Han S. Cholesterol enhances surface water diffusion of phospholipid bilayers. J Chem Phys. 2014;141:22D513.
92. Lai AL, Freed JH. HIV gp41 fusion peptide increases membrane ordering in a cholesterol-dependent fashion. Biophys J. 2014;106:172–81.
93. Stepien P, Polit A, Wisniewska-Becker A. Comparative EPR studies on lipid bilayer properties in nanodiscs and liposomes. Biochim Biophys Acta. 2015;1848:60–6.
94. Vitiello G, Falanga A, Alcides Petruk A, Merlino A, Fragneto G, Paduano L, Galdiero S, D'Errico G. Fusion of raft-like lipid bilayers operated by a membranotropic domain of the HSV-type I glycoprotein gH occurs through a cholesterol-dependent mechanism. Soft Matter. 2015;11:3003–16.
95. Lippert JL, Peticolas W l. Laser Raman investigation of effect of cholesterol on conformational changes in dipalmitoyl lecithin multilayers. Proc Natl Acad Sci U S A. 1971;68:1572–6.
96. Tantipolphan R, Rades T, Strachan CJ, Gordon KC, Medlicott NJ. Analysis of lecithin–cholesterol mixtures using Raman spectroscopy. J Pharm Biomed Anal. 2006;41:476–84.
97. Mendelsohn R. Laser-Raman spectroscopic study of egg lecithin and egg lecithin-cholesterol mixtures. Biochim Biophys Acta. 1972;290:15–21.
98. Umemura J, Cameron DG, Mantsch HH. A Fourier transform infrared spectroscopic study of the molecular interaction of cholesterol with 1,2-dipalmitoyl-*sn*-glycero-3-phosphocholine. Biochim Biophys Acta. 1980;602:32–44.
99. Gagoś M, Arczewska M. FTIR spectroscopic study of molecular organization of the antibiotic amphotericin B in aqueous solution and in DPPC lipid monolayers containing the sterols cholesterol and ergosterol. Eur Biophys J. 2012;41:663–73.
100. Xu XL, London E. The effect of sterol structure on membrane lipid domains reveals how cholesterol can induce lipid domain formation. Biochemistry. 2000;39:843–9.

101. Yasuda T, Matsumori N, Tsuchikawa H, Lonnfors M, Nyholm TKM, Slotte JP, Murata M. Formation of gel-like nanodomains in cholesterol-containing sphingomyelin or phosphatidylcholine binary membrane as examined by fluorescence lifetimes and ^{2}H NMR spectra. Langmuir. 2015;31:13783–92.
102. Iwasaki F, Suga K, Okamoto Y, Umakoshi H. Characterization of DDAB/cholesterol vesicles and its comparison with lipid/cholesterol vesicles. J Nanosci Nanotechnol. 2018;18:1989–94.
103. Sparr E, Eriksson L, Bouwstra JA, Ekelund K. AFM study of lipid monolayers: III. Phase behavior of ceramides, cholesterol and fatty acids. Langmuir. 2001;17:164–72.
104. Lawrence JC, Saslowsky DE, Edwardson JM, Henderson RM. Real-time analysis of the effects of cholesterol on lipid raft behavior using atomic force microscopy. Biophys J. 2003;84:1827–32.
105. Sacchi M, Balleza D, Vena G, Puia G, Facci P, Alessandrini A. Effect of neurosteroids on a model lipid bilayer including cholesterol: an atomic force microscopy study. Biochim Biophys Acta. 2015;1848:1258–67.
106. Warschawski DE, Devaux PF. ^{1}H-^{13}C Polarization transfer in membranes: a tool for probing lipid dynamics and the effect of cholesterol. J Magn Reson. 2005;177:166–71.
107. Holland GP, Alam TM. Multi-dimensional ^{1}H-^{13}C HETCOR and FSLG-HETCOR NMR study of sphingomyelin bilayers containing cholesterol in the gel and liquid crystalline states. J Magn Reson. 2006;181:316–26.
108. Stockton GW, Polnaszek CF, Tulloch AP, Hasan F, Smith ICP. Molecular-motion and order in single-bilayer vesicles and multilamellar dispersions of egg lecithin and lecithin-cholesterol mixtures. A deuterium nuclear magnetic resonance study of specifically labeled lipids. Biochemistry. 1976;15:954–66.
109. Brown MF. Anisotropic nuclear spin relaxation of cholesterol in phospholipid bilayers. Mol Phys. 1990;71:903–8.
110. Weisz K, Gröbner G, Mayer C, Stohrer J, Kothe G. Deuteron nuclear magnetic resonance study of the dynamic organization of phospholipid/cholesterol bilayer membranes: molecular properties and viscoelastic behavior. Biochemistry. 1992;31:1100–12.
111. Martinez GV, Dykstra EM, Lope-Piedrafita S, Job C, Brown MF. NMR elastometry of fluid membranes in the mesoscopic regime. Phys Rev E. 2002;66:050902.
112. Martinez GV, Dykstra EM, Lope-Piedrafita S, Brown MF. Lanosterol and cholesterol-induced variations in bilayer elasticity probed by ^{2}H NMR relaxation. Langmuir. 2004;20:1043–6.
113. Bunge A, Mueller P, Stoeckl M, Herrmann A, Huster D. Characterization of the ternary mixture of sphingomyelin, POPC, and cholesterol: support for an inhomogeneous lipid distribution at high temperatures. Biophys J. 2008;94:2680–90.
114. Matsumori N, Yasuda T, Okazaki H, Suzuki T, Yamaguchi T, Tsuchikawa H, Doi M, Oishi T, Murata M. Comprehensive molecular motion capture for sphingomyelin by site-specific deuterium labeling. Biochemistry. 2012;51:8363–70.
115. Ferreira TM, Coreta-Gomes F, Ollila OHS, Moreno MJ, Vaz WLC, Topgaard D. Cholesterol and POPC segmental order parameters in lipid membranes: solid state ^{1}H–^{13}C NMR and MD simulation studies. Phys Chem Chem Phys. 2013;15:1976–89.
116. Shaghaghi M, Chen MT, Hsueh YW, Zuckermann MJ, Thewalt JL. Effect of sterol structure on the physical properties of 1-palmitoyl-2-oleoyl-*sn*-glycero-3-phosphocholine membranes determined using ^{2}H nuclear magnetic resonance. Langmuir. 2016;32:7654–63.
117. Vogel A, Scheidt HA, Baek DJ, Bittman R, Huster D. Structure and dynamics of the aliphatic cholesterol side chain in membranes as studied by ^{2}H NMR spectroscopy and molecular dynamics simulation. Phys Chem Chem Phys. 2016;18:3730–8.
118. Molugu TR, Lee S, Brown MF. Concepts and methods of solid-state NMR spectroscopy applied to biomembranes. Chem Rev. 2017;117:12087–132.
119. Schmidt ML, Davis JH. Liquid disordered-liquid ordered phase coexistence in lipid/cholesterol mixtures: a deuterium 2D NMR exchange study. Langmuir. 2017;33:1881–90.
120. Ivankin A, Kuzmenko I, Gidalevitz D. Cholesterol-phospholipid interactions: new insights from surface X-ray scattering data. Phys Rev Lett. 2010;104:108101.

121. Pan J, Cheng X, Heberle FA, Mostofian B, Kučerka N, Drazba P, Katsaras J. Interactions between ether phospholipids and cholesterol as determined by scattering and molecular dynamics simulations. J Phys Chem B. 2012;116:14829–38.
122. Foglia F, Lawrence MJ, Demė B, Fragneto G, Barlow D. Neutron diffraction studies of the interaction between amphotericin B and lipid-sterol model membranes. Sci Rep. 2012;2:778.
123. Armstrong CL, Haeussler W, Seydel T, Katsaras J, Rheinstädter MC. Nanosecond lipid dynamics in membranes containing cholesterol. Soft Matter. 2014;10:2600–11.
124. Toppozini L, Meinhardt S, Armstrong CL, Yamani Z, Kučerka N, Schmid F, Rheinstädter MC. Structure of cholesterol in lipid rafts. Phys Rev Lett. 2014;113:228101.
125. McConnell H. Complexes in ternary cholesterol-phospholipid mixtures. Biophys J. 2005; 88:L23–5.
126. Stanich CA, Honerkamp-Smith AR, Putzel GG, Warth CS, Lamprecht AK, Mandal P, Mann E, Hua T-AD, Keller SL. Coarsening dynamics of domains in lipid membranes. Biophys J. 2013;105:444–54.
127. Brown MF, Thurmond RL, Dodd SW, Otten D, Beyer K. Composite membrane deformation on the mesoscopic length scale. Phys Rev E. 2001;64:010901.
128. Brown MF. Membrane structure and dynamics studied with NMR spectroscopy. In: Merz KM, Roux B, editors. Biological membranes: a molecular perspective from computation and experiment. Basel: Birkhäuser; 1996. p. 175–252.
129. Leftin A, Brown MF. An NMR database for simulations of membrane dynamics. Biochim Biophys Acta. 2011;1808:818–39.
130. Kinnun JJ, Leftin A, Brown MF. Solid-state NMR spectroscopy for the physical chemistry laboratory. J Chem Educ. 2013;90:123–8.
131. Seelig J. Deuterium magnetic resonance: theory and application to lipid membranes. Q Rev Biophys. 1977;10:353–418.
132. Seelig J, Seelig A. Lipid conformation in model membranes and biological membranes. Q Rev Biophys. 1980;13:19–61.
133. Seelig J, Macdonald PM. Phospholipids and proteins in biological membranes. ^{2}H NMR as a method to study structure, dynamics, and interactions. Acc Chem Res. 1987;20:221–8.
134. Brown MF, Chan SI. Bilayer membranes: deuterium & carbon-13 NMR. In: Harris RK, Grant DM, editors. Encyclopedia of magnetic resonance. New York: Wiley; 1996. p. 871–85.
135. Brown MF, Lope-Piedrafita S, Martinez GV, Petrache HI. Solid-state deuterium NMR spectroscopy of membranes. In: Webb GA, editor. Modern magnetic resonance. Heidelberg: Springer; 2006. p. 245–56.
136. Xu X, Struts AV, Brown MF. Generalized model-free analysis of nuclear spin relaxation experiments. eMagRes. 2014;3:275–86.
137. Rose ME. Elementary theory of angular momentum. New York: Wiley; 1957.
138. Petrache HI, Dodd SW, Brown MF. Area per lipid and acyl length distributions in fluid phosphatidylcholines determined by ^{2}H NMR spectroscopy. Biophys J. 2000;79:3172–92.
139. Thurmond RL, Dodd SW, Brown MF. Molecular areas of phospholipids as determined by ^{2}H NMR spectroscopy: comparison of phosphatidylethanolamines and phosphatidylcholines. Biophys J. 1991;59:108–13.
140. Jansson M, Thurmond RL, Barry JA, Brown MF. Deuterium NMR study of intermolecular interactions in lamellar phases containing palmitoyllysophosphatidylcholine. J Phys Chem. 1992;96:9532–44.
141. Nagle JF, Tristram-Nagle S. Structure of lipid bilayers. Biochim Biophys Acta. 2000;1469: 159–95.
142. Pastor RW, Venable RM, Feller SE. Lipid bilayers, NMR relaxation, and computer simulations. Acc Chem Res. 2002;35:438–46.
143. Huber T, Rajamoorthi K, Kurze VF, Beyer K, Brown MF. Structure of docosahexaenoic acid-containing phospholipid bilayers as studied by ^{2}H NMR and molecular dynamics simulations. J Am Chem Soc. 2002;124:298–309.

144. Klauda JB, Venable RM, MacKerell AD Jr, Pastor RW. Considerations for lipid force field development. In: Feller SE, editor. Computational modeling of membrane bilayers; 2008. p. 1–48.
145. Klauda JB, Roberts MF, Redfield AG, Brooks BR, Pastor RW. Rotation of lipids in membranes: molecular dynamics simulation, ^{31}P spin-lattice relaxation, and rigid-body dynamics. Biophys J. 2008;94:3074–83.
146. Klauda JB, Eldho NV, Gawrisch K, Brooks BR, Pastor RW. Collective and noncollective models of NMR relaxation in lipid vesicles and multilayers. J Phys Chem B. 2008;112:5924–9.
147. Klauda JB, Venable RM, Freites JA, O'Connor JW, Tobias DJ, Mondragon-Ramirez C, Vorobyov I, MacKerell AD Jr, Pastor RW. Update of the CHARMM all-atom additive force field for lipids: validation on six lipid types. J Phys Chem B. 2010;114:7830–43.
148. Venable RM, Sodt AJ, Rogaski B, Rui H, Hatcher E, MacKerell AD Jr, Pastor RW, Klauda JB. CHARMM all-atom additive force field for sphingomyelin: elucidation of hydrogen bonding and of positive curvature. Biophys J. 2014;107:134–45.
149. Gruner SM. Stability of lyotropic phases with curved interfaces. J Phys Chem. 1989;93: 7562–70.
150. Gawrisch K. Tafazzin senses curvature. Nature Chem Biol. 2012;8:811–2.
151. Brown MF, Seelig J. Influence of cholesterol on the polar region of phosphatidylcholine and phosphatidylethanolamine bilayers. Biochemistry. 1978;17:381–4.
152. Oldfield E, Meadows M, Rice D, Jacobs R. Spectroscopic studies of specifically deuterium labeled membrane systems. Nuclear magnetic resonance investigation of effects of cholesterol in model systems. Biochemistry. 1978;17:2727–40.
153. Trouard TP, Nevzorov AA, Alam TM, Job C, Zajicek J, Brown MF. Influence of cholesterol on dynamics of dimyristoylphosphatidylcholine as studied by deuterium NMR relaxation. J Chem Phys. 1999;110:8802–18.
154. Salmon A, Dodd SW, Williams GD, Beach JM, Brown MF. Configurational statistics of acyl chains in polyunsaturated lipid bilayers from ^{2}H NMR. J Am Chem Soc. 1987;109:2600–9.
155. Wiedmann TS, Pates RD, Beach JM, Salmon A, Brown MF. Lipid-protein interactions mediate the photochemical function of rhodopsin. Biochemistry. 1988;27:6469–74.
156. Petrache HI, Salmon A, Brown MF. Structural properties of docosahexaenoyl phospholipid bilayers investigated by solid-state ^{2}H NMR spectroscopy. J Am Chem Soc. 2001;123:12611–22.
157. Huber T, Botelho AV, Beyer K, Brown MF. Membrane model for the G-protein-coupled receptor rhodopsin: hydrophobic interface and dynamical structure. Biophys J. 2004;86:2078–100.
158. Shaikh SR, Kinnun JJ, Leng X, Williams JA, Wassall SR. How polyunsaturated fatty acids modify molecular organization in membranes: insight from NMR studies of model systems. Biochim Biophys Acta. 2015;1848:211–9.
159. Zurzolo C, Simons K. Glycosylphosphatidylinositol-anchored proteins: membrane organization and transport. Biochim Biophys Acta. 2016;1858:632–9.
160. Ahmed SN, Brown DA, London E. On the origin of sphingolipid/cholesterol-rich detergent-insoluble cell membranes: physiological concentrations of cholesterol and sphingolipid induce formation of a detergent-insoluble, liquid-ordered lipid phase in model membranes. Biochemistry. 1997;36:10944–53.
161. Frisz JF, Lou KY, Klitzing HA, Hanafin WP, Lizunov V, Wilson RL, Carpenter KJ, Kim R, Hutcheon ID, Zimmerberg J, Weber PK, Kraft ML. Direct chemical evidence for sphingolipid domains in the plasma membranes of fibroblasts. Proc Natl Acad Sci U S A. 2013;110:E613–22.
162. Hsueh YW, Gilbert K, Trandum C, Zuckermann M, Thewalt J. The effect of ergosterol on dipalmitoylphosphatidylcholine bilayers: a deuterium NMR and calorimetric study. Biophys J. 2005;88:1799–808.
163. Baoukina S, Rozmanov D, Tieleman DP. Composition fluctuations in lipid bilayers. Biophys J. 2017;113:2750–61.
164. Honerkamp-Smith AR, Veatch SL, Keller SL. An introduction to critical points for biophysicists; observations of compositional heterogeneity in lipid membranes. Biochim Biophys Acta. 2009;1788:53–63.

165. Heberle FA, Marquardt D, Doktorova M, Geier B, Standaert RF, Heftberger P, Kollmitzer B, Nickels JD, Dick RA, Feigenson GW, Katsaras J, London E, Pabst G. Subnanometer structure of an asymmetric model membrane: interleaflet coupling influences domain properties. Langmuir. 2016;32:5195–200.
166. McConnell HM, Radhakrishnan A. Condensed complexes of cholesterol and phospholipids. Biochim Biophys Acta. 2003;1610:159–73.
167. Ali MR, Cheng KH, Huang JY. Assess the nature of cholesterol-lipid interactions through the chemical potential of cholesterol in phosphatidylcholine bilayers. Proc Natl Acad Sci U S A. 2007;104:5372–7.
168. Pandit SA, Scott HL. Multiscale simulations of heterogeneous model membranes. Biochim Biophys Acta. 2009;1788:136–48.
169. Longo GS, Schick M, Szleifer I. Stability and liquid-liquid phase separation in mixed saturated lipid bilayers. Biophys J. 2009;96:3977–86.
170. Rog T, Orlowski A, Llorente A, Skotland T, Sylvanne T, Kauhanen D, Ekroos K, Sandvig K, Vattulainen I. Interdigitation of long-chain sphingomyelin induces coupling of membrane leaflets in a cholesterol dependent manner. Biochim Biophys Acta. 2016;1858:281–8.
171. Radhakrishnan A. Phase separations in binary and ternary cholesterol-phospholipid mixtures. Biophys J. 2010;98:L41–3.
172. Hsueh YW, Weng CJ, Chen MT, Thewalt J, Zuckermann M. Deuterium NMR study of the effect of ergosterol on POPE membranes. Biophys J. 2010;98:1209–17.
173. Miao L, Nielsen M, Thewalt J, Ipsen JH, Bloom M, Zuckermann MJ, Mouritsen OG. From lanosterol to cholesterol: structural evolution and differential effects on lipid bilayers. Biophys J. 2002;82:1429–44.
174. Greenwood AI, Tristram-Nagle S, Nagle JF. Partial molecular volumes of lipids and cholesterol. Chem Phys Lipids. 2006;143:1–10.
175. Keyvanloo A, Shaghaghi M, Zuckermann MJ, Thewalt JL. The phase behavior and organization of sphingomyelin/cholesterol membranes: a deuterium NMR study. Biophys J. 2018; 114:1344–56.
176. Williams GD, Beach JM, Dodd SW, Brown MF. Dependence of deuterium spin-lattice relaxation rates of multilamellar phospholipid dispersions on orientational order. J Am Chem Soc. 1985;107:6868–73.
177. Gross JD, Warschawski DE, Griffin RG. Dipolar recoupling in MAS NMR: a probe for segmental order in lipid bilayers. J Am Chem Soc. 1997;119:796–802.
178. Gawrisch K, Eldho NV, Polozov IV. Novel NMR tools to study structure and dynamics of biomembranes. Chem Phys Lipids. 2002;116:135–51.
179. Brown MF, Deese AJ, Dratz EA. Proton, carbon-13, and phosphorus-31 NMR methods for the investigation of rhodopsin-lipid interactions in retinal rod outer segment membranes. Methods Enzymol. 1982;81:709–28.
180. Lee AG. How lipids affect the activities of integral membrane proteins. Biochim Biophys Acta. 2004;1666:62–87.
181. Ferreira TM, Medronho B, Martin RW, Topgaard D. Segmental order parameters in a nonionic surfactant lamellar phase studied with ^{1}H-^{13}C solid-state NMR. Phys Chem Chem Phys. 2008;10:6033–8.
182. Hong M, Schmidt-Rohr K, Pines A. NMR measurement of signs and magnitudes of C-H dipolar couplings in lecithin. J Am Chem Soc. 1995;117:3310–1.
183. Kobayashi M, Struts AV, Fujiwara T, Brown MF, Akutsu H. Fluid mechanical matching of H^{+}-ATP synthase subunit *c*-ring with lipid membranes revealed by ^{2}H solid-state NMR. Biophys J. 2008;94:4339–47.
184. Seelig J. General features of phospholipid conformation in membranes. Z Physiol Chem. 1978;359:1049–50.
185. Brown MF. Theory of spin-lattice relaxation in lipid bilayers and biological membranes. ^{2}H and ^{14}N quadrupolar relaxation. J Chem Phys. 1982;77:1576–99.
186. Trouard TP, Alam TM, Zajicek J, Brown MF. Angular anisotropy of ^{2}H NMR spectral densities in phospholipid bilayers containing cholesterol. Chem Phys Lett. 1992;189:67–75.

187. Barenholz Y, Thompson TE. Sphingomyelin: biophysical aspects. Chem Phys Lipids. 1999; 102:29–34.
188. Yun-Wei C, Costa-Filho AJ, Freed JH. Dynamic molecular structure and phase diagram of DPPC-cholesterol binary mixtures: a 2D-ELDOR study. J Phys Chem B. 2007;111:11260–70.
189. Smith AK, Freed JH. Determination of tie-line fields for coexisting lipid phases: an ESR study. J Phys Chem B. 2009;113:3957–71.
190. Tong J, Borbat PP, Freed JH, Shin Y-K. A scissors mechanism for stimulation of SNARE-mediated lipid mixing by cholesterol. Proc Natl Acad Sci U S A. 2009;106:5141–6.
191. Ipsen JH, Mouritsen OG, Bloom M. Relationships between lipid membrane area, hydrophobic thickness, and acyl-chain orientational order. The effects of cholesterol. Biophys J. 1990;57:405–12.
192. Chen Z, Rand RP. The influence of cholesterol on phospholipid membrane curvature and bending elasticity. Biophys J. 1997;73:267–76.
193. Filippov A, Orädd G, Lindblom G. The effect of cholesterol on the lateral diffusion of phospholipids in oriented bilayers. Biophys J. 2003;84:3079–86.
194. Ohvo-Rekilä H, Ramstedt B, Leppimäki P, Slotte JP. Cholesterol interactions with phospholipids in membranes. Prog Lipid Res. 2002;41:66–97.
195. Ramstedt B, Slotte JP. Sphingolipids and the formation of sterol-enriched ordered membrane domains. Biochim Biophys Acta. 2006;1758:1945–56.
196. Brown MF, Thurmond RL, Dodd SW, Otten D, Beyer K. Elastic deformation of membrane bilayers probed by deuterium NMR relaxation. J Am Chem Soc. 2002;124:8471–84.
197. Brown MF. Unified picture for spin-lattice relaxation of lipid bilayers and biomembranes. J Chem Phys. 1984;80:2832–6.
198. Klauda JB, Kučerka N, Brooks BR, Pastor RW, Nagle JF. Simulation-based methods for interpreting X-ray data from lipid bilayers. Biophys J. 2006;90:2796–807.
199. Brown MF. Theory of spin-lattice relaxation in lipid bilayers and biological membranes. Dipolar relaxation. J Chem Phys. 1984;80:2808–31.
200. Nevzorov AA, Brown MF. Dynamics of lipid bilayers from comparative analysis of ^{2}H and ^{13}C nuclear magnetic resonance relaxation data as a function of frequency and temperature. J Chem Phys. 1997;107:10288–310.
201. Nevzorov AA, Trouard TP, Brown MF. Lipid bilayer dynamics from simultaneous analysis of orientation and frequency dependence of deuterium spin-lattice and quadrupolar order relaxation. Phys Rev E. 1998;58:2259–81.
202. Bloom M, Evans E. Observations of surface undulations on the mesoscopic length scale by NMR. In: Peliti L, editor. Biologically inspired physics. New York: Plenum; 1991. p. 137–47.
203. Bloom M, Evans E, Mouritsen OG. Physical properties of the fluid lipid-bilayer component of cell membranes: a perspective. Q Rev Biophys. 1991;24:293–397.
204. Althoff G, Stauch O, Vilfan M, Frezzato D, Moro GJ, Hauser P, Schubert R, Kothe G. Transverse nuclear spin relaxation studies of viscoelastic properties of membrane vesicles. II. Experimental results. J Phys Chem B. 2002;106:5517–26.
205. Althoff G, Frezzato D, Vilfan M, Stauch O, Schubert R, Vilfan I, Moro GJ, Kothe G. Transverse nuclear spin relaxation studies of viscoelastic properties of membrane vesicles. I. Theory. J Phys Chem B. 2002;106:5506–16.
206. Brown MF, Ribeiro AA, Williams GD. New view of lipid bilayer dynamics from ^{2}H and ^{13}C NMR relaxation time measurements. Proc Natl Acad Sci U S A. 1983;80:4325–9.
207. Endress E, Heller H, Casalta H, Brown MF, Bayerl TM. Anisotropic motion and molecular dynamics of cholesterol, lanosterol, and ergosterol in lecithin bilayers studied by quasi-elastic neutron scattering. Biochemistry. 2002;41:13078–86.
208. Rog T, Pasenkiewicz-Gierula M, Vattulainen I, Karttunen M. What happens if cholesterol is made smoother: importance of methyl substituents in cholesterol ring structure on phosphatidylcholine-sterol interaction. Biophys J. 2007;92:3346–57.
209. Shahedi V, Orädd G, Lindblom G. Domain-formation in DOPC/SM bilayers studied by pfg-NMR: effect of sterol structure. Biophys J. 2006;91:2501–7.

210. Endress E, Bayerl S, Prechtel K, Maier C, Merkel R, Bayerl TM. The effect of cholesterol, lanosterol, and ergosterol on lecithin bilayer mechanical properties at molecular and microscopic dimensions: a solid-state NMR and micropipet study. Langmuir. 2002;18:3293–9.
211. Yeagle PL, Martin RB, Lala AK, Lin H-K, Bloch K. Differential effects of cholesterol and lanosterol on artificial membranes. Proc Natl Acad Sci U S A. 1977;74:4924–6.
212. Bloch K. Sterol structure and membrane function. CRC Crit Rev Biochem. 1983;14:47–92.
213. Yeagle PL. Lanosterol and cholesterol have different effects on phospholipid acyl chain ordering. Biochim Biophys Acta. 1985;815:33–6.
214. Cheng K-H, Lepock JR, Hui SW, Yeagle PL. The role of cholesterol in the activity of reconstituted Ca-ATPase vesicles containing unsaturated phosphatidylethanolamine. J Biol Chem. 1986;261:5081–7.
215. Yeagle PL, Albert AD, Boesze-Battaglia K, Young J, Frye J. Cholesterol dynamics in membranes. Biophys J. 1990;57:413–24.
216. Henriksen J, Rowat AC, Brief E, Hsueh YW, Thewalt JL, Zuckermann MJ, Ipsen JH. Universal behavior of membranes with sterols. Biophys J. 2006;90:1639–49.
217. Brief E, Kwak S, Cheng JTJ, Kitson N, Thewalt J, Lafleur M. Phase behavior of an equimolar mixture of N-palmitoyl-d_{31}-D-*erythro*-sphingosine, cholesterol, and palmitic acid, a mixture with optimized hydrophobic matching. Langmuir. 2009;25:7523–32.
218. Huang JY, Feigenson GW. Monte Carlo simulation of lipid mixtures: finding phase separation. Biophys J. 1993;65:1788–94.
219. Hofsäß C, Lindahl E, Edholm O. Molecular dynamics simulations of phospholipid bilayers with cholesterol. Biophys J. 2003;84:2192–206.
220. Scheidt HA, Huster D. Structure and dynamics of the myristoyl lipid modification of Src peptides determined by ^{2}H solid-state NMR spectroscopy. Biophys J. 2009;96:3663–72.
221. Penk A, Mueller M, Scheidt HA, Langosch D, Huster D. Structure and dynamics of the lipid modifications of a transmembrane α-helical peptide determined by ^{2}H solid-state NMR spectroscopy. Biochim Biophys Acta. 2011;1808:784–91.
222. Huster D. Solid-state NMR spectroscopy to study protein lipid interactions. Biochim Biophys Acta. 2014;1841:1146–60.